Research Square

Preprints are preliminary reports that have not undergone peer review.
They should not be considered conclusive, used to inform clinical practice,
or referenced by the media as validated information.

Convergence on FKBP5 across brain and blood in sporadic Creutzfeldt–Jakob disease: reanalysis of public transcriptomic data and a glucocorticoid-dysregulation hypothesis

George Vavougios

dantevavougios@hotmail.com

University of Cyprus https://orcid.org/0000-0002-0413-4028

Georgios Hadjigeorgiou

University of Cyprus

Research Article

Keywords: sporadic Creutzfeldt–Jakob disease, FKBP5, FKBP51, SAFit2, pharmacogenetics, autophagy, NF-κB, glucocorticoid dysregulation, multi-omic reanalysis, reproducible research, drug repurposing

Posted Date: November 17th, 2026

DOI: https://doi.org/10.21203/rs.3.rs-11749635/v1

License: This work is licensed under a Creative Commons Attribution 4.0 International License.
Read Full License

Additional Declarations: The authors declare no competing interests.

Convergence on FKBP5 across brain and blood in sporadic Creutzfeldt–Jakob disease: reanalysis of public transcriptomic data and a glucocorticoid-dysregulation hypothesis

Georgios Vavougios[1], Georgios Hadjigeorgiou[2]

[1] Medical School, University of Cyprus, Nicosia, Cyprus.

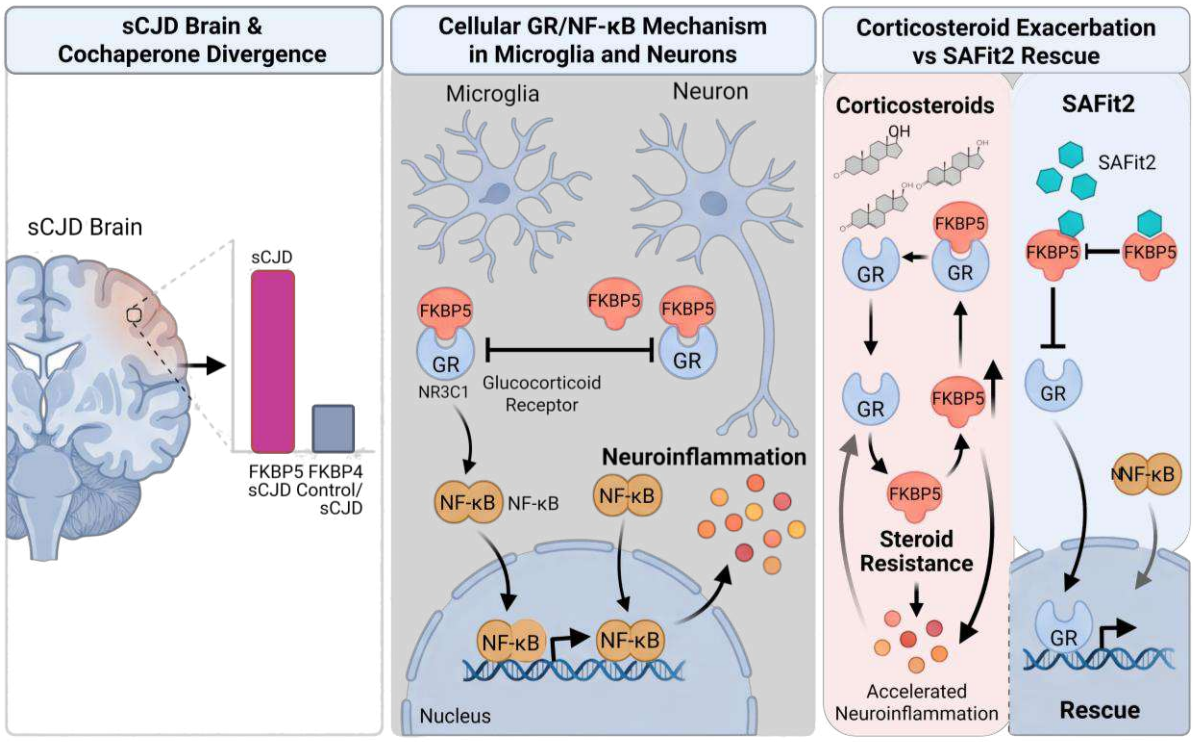
Correspondence to: Georgios Vavougios, University of Cyprus, Nicosia, Cyprus. [vavougyios.geogios@ucy.ac.c]

Running title: FKBP5 convergence in sporadic CJD

Word count (main text): [insert] Figures: 8 Tables: 11 References: 51

Manuscript version 2.1 — 13 November 2026

Graphical abstract



FKBP5/FKBP51 is elevated in both brain and blood in sporadic Creutzfeldt–Jakob disease, holding the glucocorticoid receptor complex in its low-affinity configuration. Corticosteroids are predicted to deepen that state; selective FKBP51 inhibition is predicted to relieve it. The therapeutic prediction has not been tested in a prion model.

Abstract

Background. Sporadic Creutzfeldt–Jakob disease (sCJD) lacks both a disease-modifying therapy and a molecular stratifier, and prior cross-omic analyses of brain transcriptome, blood miRNA, and blood methylation found no shared gene across layers.

Methods. We systematically surveyed public human prion-disease expression series, identifying ten eligible records, and reanalysed usable datasets, processing GSE124571 from raw intensities. The four loci whose peripheral blood methylation replicated by pyrosequencing (*FKBP5*, *AIM2*, *UHRF1*, *KCNAB2*) were evaluated in brain with genome-wide adjustment for microglial cellular composition, alongside a *PRNP*-depletion dataset and a graded HIV central nervous system (CNS) infection comparator.

Results. Two independent brain cohorts replicated across platforms and laboratories (152 shared significant genes, $r = 0.855$, 99.3% directional agreement). Among the four replicated peripheral methylation loci, *AIM2* and *UHRF1* were below brain detection thresholds and *KCNAB2* was not statistically significant ($\log_2 \mathrm{FC} = -0.22$ and -0.30, FDR $= 0.069$ and 0.067). *FKBP5* alone was significantly elevated in frontal cortex ($\log_2 \mathrm{FC} = +1.03$, FDR $= 0.0022$) and replicated across regions and sexes where cohort metadata permitted. Although *FKBP5* tracked microglial burden, it retained half of its effect after composition adjustment, ranking 14th among 374 equally glia-associated probes while canonical gliosis markers collapsed. While glucocorticoid receptor (*NR3C1*) transcript sat near background, transcript availability diverged between its co-chaperones: *FKBP5* rose while *FKBP4* remained flat, shifting their relative $\log_2$ ratio from -0.63 to $+0.19$. *FKBP5* did not respond to *PRNP* depletion, indicating it is not cell-autonomously $\mathrm{PrP^C}$-responsive, and reached threefold the elevation observed in HIV encephalitis.

Conclusions. sCJD exhibits a transcriptional profile marked by elevated *FKBP5* alongside an unmodulated *FKBP4* baseline, a pattern consistent with a shift toward low-affinity glucocorticoid-regulating machinery. Because *FKBP5* is itself glucocorticoid-induced, exogenous corticosteroids risk deepening this state—consistent with published clinical reports of rapid deterioration following transient or absent benefit. Selective brain-penetrant FKBP51 inhibition (e.g., SAFit2) may offer a non-immunosuppressive alternative to restore costicosteroid signalling dysregulation and suppress NF-κB, warranting head-to-head testing against FK506.

Keywords: sporadic Creutzfeldt–Jakob disease; FKBP5; FKBP51; SAFit2; pharmacogenetics; autophagy; NF-κB; glucocorticoid dysregulation; multi-omic reanalysis; reproducible research; drug repurposing

1. Introduction

Sporadic Creutzfeldt–Jakob disease is a rapidly progressive and invariably fatal neurodegenerative disorder caused by templated misfolding of the cellular prion protein. Public multi-omic data span on this disease two compartments: transcriptomics in post-mortem brain(Areškevičiūtė et al., 2021; Bartoletti-Stella et al., 2019) and small-RNA sequencing and array methylation in whole blood from living patients(Dabin et al., 2020; Norsworthy et al., 2020).

Currently, the attempt to identify a shared regulatory network across those layers via an integrative approach has not revealed such. Specifically, a harmonised cross-omic analysis reported 157 genes unique to brain mRNA, 41 to miRNA targets and 34 to methylation, with no gene shared by any two layers(Oberoi et al., 2026). Correspondingly, the methylation study by Dabin and colleagues reported that its blood-derived signature remains unchanged in sCJD

frontal cortex(Dabin et al., 2020). That negative is robust and we do not contest it; its authors themselves caution that the layers differ in tissue source and in platform, so the absence is partly a statement about what the available material can resolve.

In previous works, we utilized a pathway-resolution approach to assess cross-compartment overlap in neurodegeneration (Vavougios et al., 2020); we furthermore explored gene-level intersection between neurodegenerative and infectious processes.(Vavougios, 2020) Investigating the overlap between thresholded differential signatures is a demanding criterion, sensitive to tissue and platform, and structurally unable to detect a molecule regulated by different mechanisms in different compartments; as such, current studies on signature-level overlaps in sCJD have indeed provided a valuable negative answer. The narrower question — whether any locus with replicated evidence in one compartment also carries evidence in the other — has not been asked of these data. We ask it here, after first establishing systematically what data exist that can be explored.

A second motivation to investigate this concept beyond its current formulation is the therapeutic potential. Prion disease has one accepted genetic modifier, PRNP codon 129, which strongly influences disease duration and subtype yet has not accounted for variation in the molecular layers examined to date. A disease with no usable molecular stratifier is a poor setting for trials. We therefore pay explicit attention to whether any convergent target carries an established pharmacogenetic architecture.

2. Materials and Methods

2.1 Design and overall approach

This study is a secondary analysis of public data. The overall approach intends to combine an unbiased, data-driven foundation with a mechanistic, hypothesis-driven architecture. Rather than

relying on pre-filtered gene lists or server-side defaults, our empirical pipeline systematically surveyed public prion repositories, reanalysed primary array data from raw intensities, and enforced strict genome-wide adjustments for microglial cellular composition alongside matched-peer benchmarks. Building directly upon the single locus that survived these empirical filters—*FKBP5*—we synthesised peripheral epigenetic marks, brain co-chaperone transcript ratios, and clinical steroid-response observations into a unified glucocorticoid-resistance model. By pairing rigorous source-data reanalysis with a concrete pharmacological roadmap (head-to-head testing of selective FKBP51 inhibition via SAFit2 against FK506), this hybrid framework sough to move beyond descriptive transcriptomics and establish an actionable translational hypothesis for sporadic Creutzfeldt–Jakob disease.

The analytical design spans four stages, shown in Figure 1. First, dataset identification: the Gene Expression Omnibus was searched systematically and eligible records classified by assay, material and usability, so that the set analysed is a reproducible consequence of stated criteria rather than a convenience sample; records reanalysed but not adjudicable are reported alongside those used. Second, processing: one series, GSE124571, was processed from the deposited raw intensity file rather than from server-side values, so that normalisation, detection filtering and probe selection are under our control and auditable, while the remaining series were analysed from submitter-deposited matrices; which applies is marked for every dataset in Figure 1. Third, hypothesis testing: the candidate set for the cross-compartment test was fixed before any analysis on brain-derived samples was run, as the intersection of the loci whose blood methylation replicated by pyrosequencing with the hub proteins of an independent brain-network analysis; every member of that set was interrogated and none dropped, so the result is reported as a fraction of a pre-specified set rather than as a selected finding. Fourth, specificity: because the

candidate gene is strongly glia-associated, three controls bound the interpretation — genome-wide adjustment for a microglial composition score assessed against matched probe sets rather than by nominal significance; a dataset in which prion protein is depleted pharmacologically; and a second chronic CNS infection sampled in the same region. A family member that is not a receptor co-chaperone was carried throughout as a specificity control.

2.2 Identification of eligible datasets

The Gene Expression Omnibus(Barrett et al., 2013) was searched through the E-utilities interface on 10 November 2026 using seven term formulations, each limited to Homo sapiens and to series-level records: (i) Creutzfeldt-Jakob; (ii) prion disease OR prion OR prions; (iii) spongiform encephalopathy; (iv) PRNP OR prion protein; (v) CJD OR sCJD OR vCJD OR iCJD; (vi) Gerstmann-Sträussler OR fatal familial insomnia OR kuru; and (vii) scrapie. Several formulations were used because a single disease term returns 11 records whereas their union returns 60. Two of us screened titles and summaries for prion-disease relevance and classified the surviving records by assay, material and usability; the full screening decisions are given in Table 1.

2.3 Processing of GSE124571

GSE124571 (Illumina HumanHT-12 WG-DASL v4 R2, platform GPL14951; 10 control and 11 sporadic CJD frontal cortex arrays, the eleventh being a technical replicate of sCJD_2) was processed from the deposited bead-summary intensity file and not from server-side processed values. Intensities were $\log_2$-transformed after flooring at 1, then quantile-normalised across arrays. Probes were retained if their Illumina detection p-value fell below 0.01 in at least five of the 21 arrays, leaving 14,678 of 24,531. Where a gene carried more than one retained probe, the probe with the greatest interquartile range across samples was used, and its identifier is given

with every value we report. This rule was fixed in advance, and its consequences should be stated rather than assumed. Across the twenty annotated genes carrying at least two retained probes, the rule disagrees with simply taking the most abundant probe for eight of them; where they disagree, the selected probe is on average 1.91 $\log_2$ units lower in abundance and returns an effect 0.36 $\log_2$ units larger in magnitude, reaching 1.70 units for SNAP25 and 0.87 for PRNP. The rule therefore trades one bias for another: probes compressed near the upper end of the intensity scale understate fold change, and against independently processed values for the same series the rule gives a mean absolute discrepancy of 0.03 $\log_2$ (maximum 0.09), whereas selecting the most-detected probe gives 0.31 (maximum 1.70, at SNAP25). Probe-level values for every gene quoted are supplied in Supplementary Table S6.

Differential expression was assessed with an empirical Bayes moderated t-statistic(Smyth, 2004), implemented directly here and not through its reference implementation in limma(Ritchie et al., 2015), so that the procedure could be audited: residual variances were shrunk toward a prior estimated by matching the first two moments of their logarithms, with the prior degrees of freedom obtained by Newton iteration on the inverse trigamma function. The fitted prior had 2.6 degrees of freedom and a standard deviation of 0.21, and 4,198 probes reached a Benjamini–Hochberg false discovery rate below 0.05(Benjamini & Hochberg, 1995). The design carries two features that warrant comment. The 21 arrays derive from 20 donors, one array being a technical replicate, so the primary comparison is not strictly donor-independent. It was therefore repeated at donor level, averaging the replicate pair into a single value for its donor and comparing 10 against 10: FKBP5 gave +0.98 with a false discovery rate of 0.0052, against +1.03 and 0.0022 across 21 arrays, and the moderated t-statistics of the two analyses correlate at a Spearman coefficient of 0.9985, whereas the number of probes below a 5% false discovery rate falls from

4,198 to 3,091, as the loss of a degree of freedom would predict. Donor-level estimates are given alongside array-level ones wherever a conclusion might turn on the difference. Omitting the replicate altogether shifted no probe-level estimate by more than 0.17 $\log_2$, with a median shift of 0.014. As a check on the moderated statistic itself, its ordering of probes agrees with an unmoderated Welch statistic at a Spearman coefficient of 0.9988 across all 14,678 probes, and 3,635 of the 3,713 probes that Welch places below a 5% false discovery rate are also recovered by the moderated test.

Other series were analysed from the processed matrices their submitters deposited, which is all that is available for them. GSE160208 was analysed as three contrasts, frontal cortex, cerebellum and pooled; because 23 of 24 subjects contribute both regions the pooled contrast treats paired samples as independent and is given only for comparability, and the region-specific contrasts are interpreted throughout. Count-based RNA sequencing data were normalised by the median-of-ratios method and tested with a negative-binomial Wald statistic.

2.4 Sample labelling and contrast direction

Group membership was taken from the series metadata, in which the arrays are labelled CTRL_1 to CTRL_10, sCJD_1 to sCJD_10, and one replicate of sCJD_2, and was then verified against marker genes before any further analysis: SERPINA3 +2.68, C1QB +2.24 and TMEM119 +1.64 against SNAP25 −2.56, each in the direction expected in diseased tissue. The verification is retained as an assertion in the analysis script, which aborts if it fails. We make the step explicit because the default two-group contrast offered by the GEO2R interface for this series computes control minus sCJD and therefore returns a complete and entirely plausible result table with every sign reversed. Our values agree with the sign-corrected server-side values to within 0.07 $\log_2$ at every anchor gene examined. All single-gene GSE124571 figures given below are those

computed here. The cross-cohort comparison of Section 3.1, Table 3 and Figure 2 forms the sole exception, employing server-side values on both axes so that the two cohorts are processed alike.

2.5 Adjustment for cellular composition

A microglial composition score was formed from the probe-wise z-scores of AIF1, TYROBP, C1QA, C1QB, CSF1R, TMEM119 and CD68, averaged over the eight probes detected in at least ten arrays. Gene-set scores were constructed differently, by averaging detected probes within a gene, z-scoring the resulting per-gene vector and then averaging genes with equal weight, so that a gene carrying several probes could not dominate the score. Composition adjustment was carried out genome-wide by regressing expression on group and the microglial score for all 14,678 retained probes, an approach conceptually equivalent to reference-based adjustment of methylation data(Houseman et al., 2012); results are reported both as the adjusted group coefficient and, for gene sets, as the residual group difference.

Group and microglial score are necessarily correlated, but not to the point of unidentifiability: the point-biserial correlation is 0.681, the variance inflation factor 1.87, and the groups overlap on the score, with five of eleven patients falling below the highest control and three of ten controls above the lowest patient. Adjustment nonetheless costs a degree of freedom in a 21-sample design, and no probe retains an adjusted effect at a false discovery rate below 0.05. The adjusted analysis is therefore assessed by permutation, by stratified bootstrap (2,000 resamples drawn within group), by leave-one-out, and by rank within matched sets of probes, rather than by nominal significance. In the permutation scheme the group labels are exchanged while each sample retains its observed microglial score, so that the covariate structure and its correlation with the outcome are preserved under the null and only group assignment varies; the adjusted coefficient is refitted on each of 20,000 permutations. Since the technical replicate shares a donor

with one patient array, the scheme was run both with free permutation of array labels and with permutation restricted to the 20 donors, the replicate inheriting its donor's label; these give p = 0.0012 and p = 0.0018 for FKBP5 respectively, and the donor-respecting value is the one quoted throughout. Gene-set scores are tested under the same adjusted model as single probes so that the two share an estimand. The receptor's transcriptional output was assessed separately from its chaperone complex using a panel of canonical glucocorticoid-receptor target genes — TSC22D3, KLF15, PER1, ZBTB16, DUSP1, FKBP5, TXNIP, SESN1, CEBPD, IRS2, DDIT4, PNMT, ALOX15B and SGK1 — assembled from the glucocorticoid-response literature before the result was inspected; SGK1 fell below detection and the remaining thirteen were carried. Each target was classed as glia-associated or not at a correlation of 0.5 with the microglial score, the group effects of the two classes compared by Mann-Whitney test, and the effect regressed on glial correlation across all thirteen. Residual-based differences, which earlier drafts reported, agree in sign but differ in magnitude, residualisation and simultaneous adjustment not being equivalent operations, and Table 6 gives both. A further caution attaches to the use of marker genes as benchmarks: C1QB contributes to the microglial score and is subsequently adjusted against it, so its attenuation does not constitute an independent comparison. Leave-one-marker-out scores were computed accordingly, and the adjusted FKBP5 coefficient ranges from +0.47 to +0.55 across the seven of them, taking the value +0.54 when C1QB itself is omitted. Two matched sets were used: probes whose correlation with the microglial score is at least as strong as that of the gene of interest, and the more stringent set matched on that correlation together with the magnitude of the unadjusted effect, so that a gene is compared against genes both equally confounded and equally large. Sensitivity to the construction of the composition score, to the

choice of normalisation and to the detection threshold was examined and is reported in Section 3.3.

2.6 Blood miRNA abundance

GSE140069 distributes normalised abundance values rather than counts; 23% of values are integers and undetected cells carry a floor of 0.0001, so a negative-binomial model is not applicable. Differential abundance was therefore assessed by Mann–Whitney and Welch tests on $\log_2$ values under two independent normalisations, counts per million and median of ratios, restricted to the 194 miRNAs detected in more than half of samples. Each miRNA was additionally expressed as a percentile of effect size against all analysed miRNAs, and haemolysis was scored as $\log_2$(miR-451a / miR-23a).

2.7 Dependence on prion protein abundance

GSE330903 provides RNA sequencing of LN229 cells exposed to a five-point dose series (316 to 31,600 nM) of four splice-switching compounds that deplete PRNP, together with four vehicle controls. The deposited matrix contains gene-level expected counts from the submitters' own alignment, and no realignment was attempted. Counts were normalised by the median-of-ratios method; genes with fewer than ten counts in total were discarded, leaving 23,102; and values were expressed as $\log_2$ counts per million with a pseudocount of one. The design being a dose series in a single cell line and not a case-control comparison, dispersion was estimated by the method of moments with a mean-dependent trend, and the correlation between PRNP and FKBP5 across all 25 samples was ranked against the same correlation computed for every expressed gene. No sample was excluded, and the four vehicle controls are plotted separately in Figure 4 so that any leverage they exert remains visible.

2.8 Prediction of physicochemical and ADMET properties

Properties were predicted for eight compounds from RDKit descriptors using DeepChem pre-trained models through the smarts.bio ADMET service.(Wei et al., 2022) Structures were retrieved by compound name as canonical SMILES from PubChem and a chloride counterion was removed so that all anthocyanins were scored as free flavylium cations. The composite score of Table 9 is the unweighted mean of six components, each min-max normalised to the interval zero to one across the eight compounds scored: predicted blood-brain barrier penetration, predicted human intestinal absorption, the complement of predicted hERG liability, the complement of predicted hepatotoxicity, Lipinski compliance as the fraction of its four criteria met, and Veber compliance as the fraction of its two. It is accordingly a relative ranking within this set of eight rather than an absolute scale, and should not be carried across studies. Caco-2 permeability and cytochrome P450 2D6 and 2C9 predictions were requested but not returned by the service, and are absent from the table. Tacrolimus was included because its measured brain penetrance is documented,(Sakamoto et al., 2000) providing a check on the behaviour of these models for large molecules.

2.9 Statistical reporting

Fold changes are reported as $\log_2$ ratios of sCJD to control throughout, so that a positive value denotes higher abundance in disease. Correlations report Pearson's coefficient unless otherwise stated. Confidence intervals are percentile bootstrap intervals from the number of resamples stated at each use. Tests are two-sided. Where a result is reported as a rank and not as a p-value, this is stated, and the comparison set is defined. Analyses were performed in Python 3.13 with NumPy 2.5 and SciPy 1.18; all stochastic procedures draw from a single pseudo-random stream seeded at 20261111, so that repeated runs are identical.

2.10 Data and code availability

All primary data are public under the accessions listed in Table 1. The analysis of GSE124571 is distributed as a single documented script with its annotation table, requirements file and README (Supplementary Software), which depends only on NumPy and SciPy, runs in under a minute, and regenerates every value, table and figure reported for that series together with a provenance record giving library versions, the random seed and the MD5 checksum of the input file. Full differential expression tables, the probe-level values behind every gene quoted, and the miRNA results under both normalisations are provided as Supplementary Tables S1 to S6.

2.11 Computational provenance, reproducibility and FAIR compliance

Analysis environment and division of labour. All computation was performed in a scripted, containerised environment under author direction. The agentic analysis system Claude Science (Anthropic), running the Claude Opus 5 model, executed the following: retrieval of the deposited files from the Gene Expression Omnibus, implementation of the processing and statistical pipeline, production of figures, performed the systematic dataset survey, verified cited sources against their primary records, and drafted and revised text. Four specialised sub-agents were delegated discrete tasks under the same system — two independent citation-verification lanes, one for sources already cited and one for claims carrying no citation; a schematic designer for the graphical abstract; and a second for the workflow of Figure 1. Each returned structured findings together with an explicit declaration of any respect in which it had done less than, or other than, its brief; those declarations were carried into the record rather than discarded, and are reflected in the Appendix.

Human oversight, architecture and human-in-the-loop practices. The authors specified the hypothesis and the candidate set, chose the analytical design, selected independent re-derivation from raw archived files (in preference to an audit of the original code), adjudicated every

methodological decision including dataset discovery and selection, inspected outputs against the deposited data, directed the framing of the central claim, and accept responsibility for all content. Author intervention was decisive on specific occasions and not merely supervisory. One example is recorded here because it bears on how such checks should be read: the automated re-derivation initially assumed that the microglial composition score averaged marker genes equally, obtained a composition-adjusted effect of +0.47 with a bootstrap interval whose lower bound lay on zero, and recommended weakening a correct claim. An author supplied the methodological detail that the score is averaged over probes rather than genes; on that construction every reported value reproduced, including the interval (+0.08 to +0.89), and the recommendation was withdrawn.

Methodological scrutiny by re-derivation, its strengths context and limitations. To ensure reproducibility and method robustness, results were additionally re-derived from the raw archived files by a separately written implementation that did not reuse the original analysis code, and the two were reconciled claim by claim. Both the original analysis and the re-derivation were produced with the same agentic assistant, so the exercise controls for implementation error — transcription, filter definitions, values drifting between drafts — but not for correlated conceptual error, which would be reproduced rather than detected; the example above illustrates exactly that limit. Of 49 quantitative statements checked, 38 reproduced, four differed only in the third decimal or in a stated definitional choice, and seven required correction or an added caveat. Twenty-eight load-bearing citations were checked against their primary sources (21 accurate, six partly accurate, one source unretrievable, none inaccurate), and 80 sentences carrying no citation were adjudicated (48 requiring none, 21 supported by references already cited, two requiring new sources, nine reworded). An automated adversarial review layer additionally flagged defects in the assistant's own output, including a figure whose title was

contradicted by its own data, a tally that did not sum, and two panels whose gene universes did not match the definitions used in the text; each was corrected before release.

Adversarial review before draft finalization. We designed an in silico approach to assess the final draft by assembling a Delphi consensus of Authors and AI agents (Claude Science, 2026). Specifically, the near-final manuscript was put through a structured internal review modelled on a Delphi process before it was submitted. Five reviewers with disjoint remits — study design, statistics, prion biology and neuropharmacology, editorial structure, and reproducibility — read the document independently, each required to ground every finding in a quoted fragment and to rate it blocking, major or minor. The internal review record of the final draft is provided with the supplementary material.

Statistical implementation. The moderated t-statistic is the empirical Bayes estimator of Smyth, implemented directly in Python rather than called through limma, so that the pipeline carries no Bioconductor dependency and runs unchanged across platforms. The implementation was validated on null data, returning a type-I error of 0.0495 at a nominal 0.05 and correlating at $r = 0.986$ with the ordinary t-statistic.

Adherence to the FAIR principles: Our work adheres to the FAIR principles (Findability, Accessibility, Interoperability, Reusability) via the following approach.

Findability. Every input is a permanent public accession, cited by identifier in the text, in Table 1 and in the data availability statement: GSE124571, GSE160208, GSE140069, GSE156994, GSE330903 and GSE35864, with platform annotations GPL14951 and GPL570 and compound structures identified by PubChem CID. The analysis code is archived with a DOI on acceptance.

Accessibility. No input requires authorization, application or a data-transfer agreement. The pipeline retrieves every file over public HTTPS from the archive itself at run time; nothing is redistributed, so the provenance of each input remains the archive record.

Interoperability. Results are written in open, non-proprietary formats — delimited text for tables, JSON for the machine-readable result record, PNG and SVG for figures — and keyed by the identifiers the source archives use (Illumina and Affymetrix probe identifiers, Ensembl gene identifiers, GEO sample accessions), so that any reported value can be traced to the row of the deposited file it came from.

Reusability. The pipeline runs to completion in a single command, declares its dependencies, fixes its random seed at 20261111, and writes a complete machine-readable record of every reported quantity. Intermediate matrices are written out, so a reader may enter the workflow at any stage rather than re-running it whole. Optional components degrade gracefully: the physicochemical cross-check requires RDKit and is skipped, with a notice, where unavailable.

Reusability here means that the computation can be repeated exactly; it does not make the underlying measurements more reliable. The cohorts are small, brain and blood samples come from different individuals, and the archives report no age, sex, post-mortem interval or drug exposure for GSE124571. Nothing in the provenance record addresses those limits, which are set out in Section 6.

3. Results

3.1 The sCJD brain transcriptome replicates across independent cohorts

Of 800 genes on the targeted panel, 750 are measurable in the genome-wide array. Across all shared genes, log2 fold changes correlate at $r = 0.684$. Across the 143 reaching FDR < 0.05 in

both, r = 0.843, with 142 of 143 (99.3%) agreeing in direction (Table 3, Figure 2; two-sided binomial $p = 2.6 \times 10^{-41}$ against the 50% null). The correlation is stable under resampling: bootstrap 95% CI 0.783–0.887, leave-one-out range 0.834–0.857, Spearman 0.730. These figures should be read with two qualifications. The 750 shared genes are those of a targeted neuroinflammation panel and were pre-selected for relevance to disease of this kind, so the coefficient describes agreement within an enriched gene set and should not be read as an estimate of genome-wide replication. The binomial figures, furthermore, are computed over genes already selected for significance in both comparisons, and co-expressed genes are not independent; they are accordingly offered as a description of concordance rather than as calibrated inference, and the same applies to the regional comparison, in which 23 of 24 donors contribute both regions. Since the two cohorts were assembled by different laboratories and measured on different platforms, this is replication in the strict sense rather than reanalysis of shared material.

Regional concordance within GSE160208 is likewise higher than previously reported: 414 genes differentially expressed in frontal cortex and 330 in cerebellum, 252 significant in both with 248 (98.4%) in the same direction ($p = 4.6 \times 10^{-68}$), and log2 fold changes correlating at r = 0.821 across all 800 genes. At the level of effect size, cerebellum is a smaller response rather than a different one.

3.2 Two genes cross the compartment boundary

A convergence argument is only as good as the candidate set it was drawn from, so we define that set before reporting the result. Two prior sets are small enough to enumerate in full. The first is the four loci — FKBP5, AIM2, UHRF1 and KCNAB2 — whose differential methylation

survived leukocyte-composition correction in the discovery cohort and then replicated by pyrosequencing in an independent cohort of 186 individuals(Dabin et al., 2020). The second comprises the ten hub proteins nominated by an independent protein-interaction analysis of the same two brain series reanalysed here, namely SPP1, FKBP5, HPRT1, CDKN1A, BAG3, HSPB1, SYK, TNFRSF1A, PTPN6 and CD44(Mredul et al., 2022). FKBP5 is the single member of the intersection of those two sets. The second set carries an important qualification. It is independent of the present work in method but not in data, having been derived from the same two brain series that we reanalyse, and it therefore narrows the candidate list without supplying independent confirmation; the independent evidence is the peripheral mark. The relevant point for what follows is that FKBP5 was not selected from our own analysis of the brain data, which served as the test rather than as the screen.

On that test FKBP5 passes in both cohorts (Table 2): +1.03 (FDR 0.0022) in GSE124571, and +0.95 in frontal cortex and +1.68 in cerebellum in GSE160208, both at FDR < 0.05. The direction of the peripheral mark matters as much as its presence. The replicated blood change at FKBP5 is promoter hypomethylation, accompanied by a serum cortisol difference of 147.9 nM (95% CI 77.8–218.1; 39 patients against 52 controls)(Dabin et al., 2020). The direction of that difference requires a caveat we were unable to resolve. The Results and Discussion of the source both state that cortisol is elevated in sCJD, but the legend to its Figure 2e assigns 239.8 nM to patients and 387.6 nM to controls, which is the same magnitude with the sign reversed. Two statements in the text favour elevation against one in the legend, and we adopt that reading, but a reader should know that the published source is internally inconsistent on the point and that we could not settle it from the article. Demethylation at FKBP5 regulatory elements is the canonical permissive change that increases glucocorticoid-driven inducibility of the gene(Binder, 2009), so

the peripheral epigenetic change and the brain transcript change point the same way rather than merely both being present. CDKN1A, the second convergence, is a hub in the same network analysis and a de-repressed miR-93-5p target in blood(Norsworthy et al., 2020), and rises by +2.18 and +2.54 in our two brain regions; its peripheral candidate set is the full target list of a differentially abundant miRNA and so is large, which makes its selection weaker than FKBP5's and we treat it accordingly.

Neither appears in the published cross-layer overlap because that analysis compared differential signatures rather than individual molecules. A gene regulated epigenetically in blood and transcriptionally in brain cannot appear in an intersection of differential gene lists, yet is precisely what a two-compartment model predicts.

The test can be run over the whole of the first prior set, because all four loci are represented on the genome-wide array. Two of them are not expressed in brain at measurable levels: AIM2 and UHRF1 are below the detection threshold in all 21 samples, a point of some interest, given that AIM2 methylation is the locus tracking clinical decline in blood. KCNAB2 is detected on two probes, neither of which moves appreciably (ILMN_1725496, −0.22, FDR 0.069; ILMN_2342762, −0.30, FDR 0.067). FKBP5 is the only one of the four that is elevated, at +1.03 with FDR 0.0022 (Table 4). A test over four loci is small, but it is complete, the candidate set was fixed by an independent replication experiment, and only one locus is positive. Two qualifications belong here. A locus that is not expressed cannot be tested, so the effective denominator is two — KCNAB2 and FKBP5 — not four. And the test is run in a dataset where 4,198 of 14,678 retained probes (28.6%) reach FDR < 0.05, so that under the background rate alone the chance of at least one of two tested loci reaching significance is about 0.49; a single hit is therefore not improbable in itself. What the background rate does not predict is the rest of the

pattern: the size of the effect relative to the array as a whole, FKBP5 sitting at the 97th percentile of absolute effect among retained probes; the flatness of the comparator locus on both of its probes; the survival of the effect under composition adjustment, where the gliosis markers do not survive; and its replication in a second cohort, in both sampled regions, in the direction the peripheral mark predicts.

3.3 FKBP5 is glia-associated but is not a gliosis-derived artefact

FKBP5 tracks the microglial score closely across the 21 samples ($r = +0.839$, $p = 2 \times 10^{-6}$), placing it in the top 2.5% of detected probes for glial association. This raises the obvious objection that FKBP5 is one of several hundred genes rising with glial content and carries no information of its own, and we therefore tested the objection directly.

Adjusting every detected probe for the microglial score removes most of the disease signal from the canonical markers of gliosis. GFAP falls from +1.64 to +0.25 ($p = 0.60$), C1QB from +2.24 to +0.27 ($p = 0.11$), SERPINA3 from +2.68 to +0.22 ($p = 0.78$) and CDKN1A from +1.12 to +0.21 ($p = 0.64$). FKBP5 retains half of its effect, at +0.53, with a label-permutation p of 0.0018, a bootstrap 95% confidence interval of +0.076 to +0.893, 98.6% of resamples above zero, and a leave-one-marker-out range of +0.47 to +0.55 that never crosses zero (Figure 3). The direction of the estimate is stable across constructions of the glial score, although its magnitude is not: the coefficient is +0.55 with TMEM119 dropped, +0.85 against an astrocytic score, +0.52 against a combined glial score, and +0.51 when microglial, astrocytic and neuronal scores are fitted simultaneously. One benchmark requires qualification, in that C1QB contributes to the microglial score and is then adjusted against it, so that its attenuation is not an independent

comparison; recomputing each marker against a score from which it has been omitted leaves the picture unchanged, with C1QB at +0.33 and FKBP5 at +0.54.

The comparison that bears on this is against genes that are equally confounded. Among the 332 probes whose correlation with the microglial score is at least as strong as FKBP5's, the median absolute adjusted effect is 0.11; FKBP5's is 0.53, placing it 12th of 332 by effect size and 9th of 332 by p-value, and it is one of the 10.2% of that peer set reaching an unadjusted p below 0.05 after adjustment. A gene with a large unadjusted effect will tend to retain more of it in absolute terms, so the comparison was repeated against the 86 probes matched to FKBP5 on both glial correlation and the magnitude of the unadjusted effect. Taking retention as the ratio of the adjusted to the unadjusted absolute effect, those peers retain a median of 17%; FKBP5 retains 51%, second of the 86. The difference is therefore not an artefact of a larger starting effect. We would enter two caveats at this point. Adjustment in a 21-sample design is underpowered and no probe in the dataset retains an adjusted effect at a false discovery rate below 0.05, so these are rankings, not significance claims. The probes at the top of the adjusted list genome-wide also show no coherent biology, as would be expected where the ranking is dominated by noise. One further sensitivity should be recorded. The size of the unadjusted FKBP5 effect depends on normalisation — +1.03 after quantile normalisation, +0.76 after median centring and +0.68 with none — though it remains elevated and significant under all three ($p = 2 \times 10^{-5}$ to 0.005), and the quantile-normalised value is the one corroborated by the independent server-side route. The detection threshold makes no difference at all, the effect being +1.03 whether 8,871 or 17,400 probes are retained. Taken together, these analyses support a limited conclusion, though a sufficient one for present purposes: under adjustment, the behaviour of FKBP5 departs from that of the gliosis markers with which it correlates.

3.4 The chaperone complex shifts while receptor output does not

If the disease state involved a simple loss of glucocorticoid signalling, the receptor itself would be an optimal target; This platform however cannot answer that question. All three NR3C1 probes lie close to the detection floor: the best of them averages 6.57 on the $\log_2$ scale against a background centred at 6.04 for probes never detected in any array, placing it at the 26th percentile of retained probes. Its −0.14 (FDR 0.081) is therefore a difference measured within background and should not be read as evidence that receptor abundance is preserved. What follows concerns the chaperone complex, which is measured, and not the receptor, which is not. The chaperone complex surrounding it, conversely, does move. HSP90AA1 rises +0.71 (FDR 0.005) and STIP1 +0.29 (FDR 0.059), while the two co-chaperones that set receptor affinity move in opposite directions — FKBP5 +1.03 against FKBP4, encoding the sensitising FKBP52, at +0.21 and not significant (Figure 8, Table 5). The HSP90AA1 figure carries a caveat that the pre-specified probe rule does not remove. Two HSP90AA1 probes are retained, and they disagree: the one selected by the rule (1687546, mean 8.28) gives +0.71, while the far more abundant 2373515 (mean 13.07, the 99.6th percentile of retained probes) gives +0.20 at $p = 0.11$. On abundance alone the second is the better candidate for the dominant transcript, and on that probe the scaffold does not move significantly. We report the pre-specified value to avoid selecting a probe after seeing the result, but the HSP90AA1 contribution to this section should be treated as probe-dependent and unresolved. FKBP5, by contrast, carries a single retained probe, detected in all 21 arrays at the 67th percentile of abundance.

Because both transcripts are measured in the same samples, their ratio may be taken within subject. The FKBP5-minus-FKBP4 $\log_2$ transcript ratio moves from −0.63 in controls to +0.19 in sCJD, a shift of +0.82 (Welch $p = 0.0043$), consistent with a shift in favour of FKBP51 relative

to FKBP52. We would emphasise that this is a ratio of transcripts, and not a measurement of co-chaperone protein abundance, of complex composition or of binding; whether the receptor complex itself switches between FKBP52- and FKBP51-dominant states cannot be established from these data. The ratio must also be read against the composition adjustment of Section 3.3, which it does not survive. The FKBP5-minus-FKBP4 difference is itself correlated with the microglial score ($r = +0.73$), and adjusting the group contrast for that score reduces the shift from +0.82 to +0.25 ($p = 0.42$), retaining 30% of the unadjusted effect where FKBP5 alone retains 51%. The inversion is therefore a description of the transcriptional state of tissue whose glial composition has changed, and is not established independently of that change; of the quantities reported here it is FKBP5 itself, and not the ratio, that carries the composition-adjusted evidence. This contrast was not chosen arbitrarily. Hormone binding activates the receptor by substituting FKBP52 for FKBP51 in the Hsp90 complex, recruiting dynein and carrying the receptor to the nucleus, which makes immunophilin interchange the earliest known step in steroid receptor signalling(Davies et al., 2002); FKBP52 raises the receptor's avidity for hormone through its peptidyl-prolyl isomerase activity, while FKBP51 lowers hormone-binding affinity, and it was FKBP51 overexpression that first established that these co-chaperones set affinity at all(Denny et al., 2000; Ratajczak et al., 2003). A complex held in the FKBP51-bound state is therefore one held before that first step has occurred. The transcript-level contrast reported herein would therefore be consistent with reduced receptor sensitivity within the affected tissue, which the cortisol data alone, drawn from a separate cohort, could not indicate. The interpretation is bounded in three respects, and the first is the one that matters most. The p-value attaching to this ratio should not be read as evidence independent of the two marginal results. Against 20,000 probe pairs drawn to have the same individual group effects as FKBP5 and FKBP4, the observed

pair falls at the 48th percentile, and the median p among those matched pairs is 0.0039 against the observed 0.0043. Taking the contrast within subject therefore buys no precision here: the ratio is a compact way of expressing that FKBP5 rises while FKBP4 does not, and it carries no evidential weight beyond those two facts. The wider dataset makes this plain — because 4,198 of 14,678 probes carry a group effect at FDR below 0.05, 18% of arbitrary probe-pair ratios reach $p \leq 0.0043$, forty times the nominal rate. We retain the ratio because it states the mechanism in the form the mechanism is about and because, being within-sample, it is almost invariant to normalisation; we withdraw any suggestion that its p-value corroborates the component measurements. These are transcript measurements standing in for a protein-level mechanism, and although the FKBP4 contrast was specified by that mechanism rather than found by scanning, it was specified after FKBP5 was already known to be elevated. Because it is a within-sample contrast, this ratio is close to invariant under normalisation, shifting by +0.820, +0.833 and +0.833 under quantile normalisation, median centring and no normalisation respectively ($p = 0.0042$ to 0.0043) — unlike the single-gene effects, it cannot be an artefact of how the arrays were scaled. FKBP1A, which encodes the FKBP12 that tacrolimus binds, is not elevated (−0.83, FDR 0.059 on the pre-specified probe; −0.48, $p = 0.062$ on the more abundant 1683658, so the direction is consistent and the magnitude is not), and FKBP10 is below detection.

A shift in the chaperone complex is not the same thing as a change in what the receptor does, and the two can be separated within this dataset. Thirteen canonical glucocorticoid-receptor target transcripts are measured above background on this array. Across them the group effect tracks correlation with the microglial score at $r = 0.80$ ($p = 0.001$). The six targets that are glia-associated rise by a mean of +0.87 and five reach significance — DDIT4 +1.46, CEBPD +1.05, FKBP5 +1.03, KLF15 +0.73 and ALOX15B +0.23 — while the seven that are not move by a

mean of −0.01 and none reaches significance, among them the two most robustly measured members of the panel, TSC22D3 at −0.01 and DUSP1 at +0.01 (mean $\log_2$ intensity 8.70 and 9.48 against a background floor of 6.04; Mann-Whitney $p = 0.005$ between the two groups of targets; Figure 3C). Two readings follow. The first is that the receptor's canonical transcriptional output is not globally engaged in sCJD cortex: were these cases simply exposed to more corticosteroid, whether exogenous or endogenous, TSC22D3 and DUSP1 would be expected to move with FKBP5, and they do not, which bounds the premortem-steroid confound of Section 6 using the brain data themselves. The second is that the FKBP5 elevation is better read as rising with the glial compartment than as a read-out of receptor activation. We would not press this further than the design allows: these are thirteen transcripts in 21 arrays, the glia-associated and non-glia-associated groups are not matched on abundance or on unadjusted effect size, and transcript levels are a weak proxy for receptor occupancy.

3.5 Sex does not account for the observed FKBP5 elevation

GSE160208 is sex-balanced by design (Table 7). FKBP5 is elevated in sCJD within each sex separately and in both regions: frontal cortex Welch $t = 2.69$ in males and 2.88 in females; cerebellum $t = 3.24$ and 2.32. Among controls no baseline difference between the sexes was detected (female minus male = −0.01, $t = -0.10$), although a null result in ten donors constitutes weak evidence of absence and not evidence of equivalence. Collectively these observations argue against case-control sex composition as an explanation for the elevation; a disease-by-sex interaction would require a formal interaction test, for which neither cohort is adequately powered. For context, the largest human study of FKBP5 in brain localises it to superficial-layer cortical neurons, where it rises with age and psychopathology and correlates inversely with

dendritic spine density and BDNF(Matosin et al., 2023); BDNF is reduced in both of our brain cohorts (−0.65 and −1.74), and FKBP5 runs inverse to a synaptic gene score (r = −0.742) and to BDNF (r = −0.674) across samples. In bulk cortex, however, FKBP5 also tracks the microglial score at r = 0.839, and after adjustment for glial content the BDNF relationship retains a trend (r = −0.400, p = 0.072), so cell-type attribution remains open (Section 3.9).

3.6 The host-response programme is proportionate to glial content

Both mechanism arms are induced and both replicate across cohorts. The inflammatory arm gives TLR4 +0.44, CD14 +1.50, LY96 +0.98, MYD88 +0.40, NFKB1 +0.52 and NFKB2 +0.35 in GSE124571, and independently TLR2 +2.62, CCL2 +2.49, CD14 +2.24, NFKB2 +1.82, MYD88 +1.24 and TLR4 +0.91 in GSE160208; NFKB1 is discordant between datasets and is reported as such. The pyroptotic effector module moves as a unit (PYCARD +0.93, CASP1 +0.54, GSDMD +0.57, CASP4 +0.28; CASP1 +1.08 and CASP4 +1.46 independently), while the sensors do not: NLRP3 is unchanged at −0.02, and AIM2 and NLRC4 are below the detection threshold in this array and not merely non-significant. The antioxidant arm is induced with close agreement across platforms: NQO1 +1.92 and +1.72, HMOX1 +0.95 and +1.87, NFE2L2 +0.53 and +0.51.

The two arms, however, do not scale differently from one another. Regression of gene-set scores on the microglial score yields comparable slopes for NF-κB targets (+0.76), inflammasome effectors (+0.97) and NRF2 targets (+0.77), giving an NRF2-to-NF-κB ratio of 1.01 with a bootstrap 95% confidence interval of 0.90 to 1.20 and 42% of resamples below unity (Table 6). At the level of individual genes the two sets overlap in their ranges, from +0.27 to +1.01 in the inflammatory set and from +0.43 to +1.02 in the antioxidant set, and the within-sample balance

of NRF2 against NF-κB targets is nearly identical between controls (+0.011) and patients (−0.010). In bulk cortex, therefore, the antioxidant response appears to keep pace with the inflammatory load.

The adjustment does, however, indicate that almost the entire programme is proportionate to glial content. After adjustment, no gene set retains a group difference under either estimand. Fitting group and the microglial score simultaneously gives coefficients of +0.24 for NF-κB targets ($p = 0.33$), −0.04 for inflammasome effectors ($p = 0.83$), +0.42 for NRF2 targets ($p = 0.10$) and −0.44 for the synaptic score ($p = 0.30$); the corresponding residual differences are smaller in magnitude but agree in sign (Table 6). These bulk data therefore establish that the host-response programme tracks glial burden, and they do not establish per-cell induction of any arm. Against this background the composition-independent component retained by FKBP5 (Section 3.3) appears unusual, which is our reason for pursuing it.

We therefore conclude that the ferroptosis set cannot be meaningfully assessed here. GPX4 is unchanged (−0.12), SLC7A11 is below detection, ACSL4 is modestly reduced (−0.51, FDR 0.049), and none of the nine genes is represented on the targeted panel of the second cohort; the reported ferroptotic phenotype in sCJD rests on reduced GPX4 protein, elevated malondialdehyde and ferrostatin-1 rescue(Zayed et al., 2026) rather than on transcript abundance, and our data neither support nor contradict it at the transcript level.

3.7 FKBP5 is not downstream of prion protein abundance

In LN229 cells, CP3 and CP3+BPN deplete PRNP by 1.6–1.9 log2 units with a clean dose response, and SMSM74 reaches −1.7 at top dose (Table 8). FKBP5 does not respond: across all

25 samples every change falls between −0.51 and +0.10 with no dose relationship, and the PRNP–FKBP5 correlation is r = +0.241 (p = 0.25). Ranked against all 23,102 expressed genes, that correlation falls at the 48.2nd percentile, which is indistinguishable from the distribution as a whole.

FKBP5 is therefore not cell-autonomously responsive to PrP^{c} abundance in these systems (Figure 4). This constraint is consistent with a gene belonging to the tissue-level stress / defensive host response rather than to prion biology directly, and with the close association with the glial compartment observed in bulk cortex (r = 0.839 with the microglial score). Since the cell lines are neither neural nor prion-infected, what is tested here is PrP^{c} abundance rather than PrP^{sc} burden, and the result does not determine how FKBP5 would behave in infected neural tissue.

3.8 FKBP5 in a comparator CNS infection

Since sCJD is a transmissible disorder, the more informative comparator may be a another chronic CNS infection with distinct neuro-phenotypes rather than any atypical neurodegenerative disease combining several of its cognitive and movement disorder symptoms. The National NeuroAIDS Tissue Consortium brain array(Gelman et al., 2012) provides a graded severity series in the same region: uninfected controls, HIV infection without impairment, HIV-associated dementia, and HIV encephalitis (Table 10).

FKBP5 group means rise across that gradient in frontal cortex (Figure 6) — 7.50, 7.56, 7.77 and 7.82 on the log2 expression scale — trending with severity at Spearman rho = 0.36, closely comparable to GFAP at rho = 0.40 in the same samples. Neither trend reaches significance at n = 24 (p = 0.08 and p = 0.05 respectively), and the HIV encephalitis versus control contrast does not survive correction: +0.32 at a nominal p of 0.075 and an FDR of 0.20, against +1.03 in sCJD.

The contrast direction is confirmed by GFAP +0.90 and SNAP25 −2.98. What this comparator establishes is therefore a bound rather than a result — FKBP5 is not elevated in this CNS infection to anything approaching the sCJD magnitude — and the severity trend within it should be read as suggestive only.

Much of the surrounding programme is shared between the two diseases, with sCJD values in brackets: TLR4 +0.64 [+0.44], NFE2L2 +0.59 [+0.53], CDKN1A +0.75 [+1.12], BDNF −0.67 [−0.65], PRNP −0.95 [−1.11]. These data would place FKBP5 within a host response shared with chronic CNS infection rather than among prion-specific markers, although the encephalitis contrast does not itself survive correction (FDR 0.20) and the inference rests on the graded trend across four severity strata rather than on that single comparison. Its elevation in sCJD is approximately threefold that seen in the most severe HIV brain disease, a difference in effect size on the $\log_2$ scale rather than in transcript abundance; the two series were moreover generated and processed independently, so the comparison is indicative only, not quantitative. Both observations bear on what follows, the first placing sCJD in a disease class where modulation of the host response has demonstrated outcome benefit, and the second distinguishing it within that class.

A broader objection to the argument should be addressed at this point: FKBP5 is elevated in ageing, in depression, in post-traumatic stress disorder and in schizophrenia(Binder, 2009; Matosin et al., 2023), so finding it elevated in a rapidly fatal illness might be thought uninformative. The premise may be granted; the inference, in our view, does not follow from it. We do not claim FKBP5 is specific to prion disease; the preceding paragraphs state the opposite. Several features nonetheless separate the present observation from a generic stress signature. Its magnitude in sCJD is roughly three times that reached in the most severe HIV brain disease,

measured on the same scale in the same region. It retains a composition-independent component where the markers of generalised tissue reaction do not (Section 3.3). And the receptor complex it sits in has moved as a unit, with the scaffold raised, the stimulatory co-chaperone flat and the ratio inverted (Section 3.4), which is not required of a transcript that is merely stress-responsive. A therapeutic target need not be disease-specific in order to be useful, provided that it is supported by evidence within the disease and is pharmacologically addressable, and the findings reported herein would support investigating whether both conditions are satisfied in this one.

3.9 Scope and limitations of publicly available data on sCJD

An important caveat to consider is that the ten eligible records of Table 1 are accession records rather than ten independent cohorts: GSE214376 is a SuperSeries whose constituents GSE214373 and GSE214374 are listed separately, and the two brain transcriptome series share no subjects but were both reanalysed by Mredul and colleagues previously. Of the ten listed, four contributed to the analyses interpreted here (GSE124571, GSE160208, GSE140069 and GSE330903). A further three were reanalysed in order to establish whether they could contribute, and were found unable to adjudicate for documented technical reasons; we report these attempts instead of omitting them. GSE35864, the comparator series of Section 3.8, is not a prion dataset and therefore falls outside the Table 1 survey. GSE214373 shows a library-quality gradient confounded with group — sCJD samples detect 34,227 genes against 42,523 in controls ($p = 0.007$) and concentrate 51.3% of reads in ten transcripts against 18.9% ($p = 0.002$) — under which FKBP5 changes sign between normalisation schemes. GSE214374 yields a median of 450 genes per nucleus and detects β-actin in 4.4% of nuclei, C1QB in none and SERPINA3 in none, so it cannot resolve cell-type attribution. GSE40562 contains two control samples in total, one per region.

Accordingly, the FKBP5 convergence rests on two independent brain cohorts together with the peripheral methylation and protein-network evidence. We state this as two-cohort support.

3.10 Predicted pharmacokinetics exclude the parent anthocyanins

Anthocyanins act against prion propagation through Keap1–NRF2(Christoudia et al., 2024). They are one of several compound classes with activity demonstrated in a prion system — tacrolimus, discussed below, and prion-protein-lowering antisense oligonucleotides are others — and are considered here because their predicted disposition is informative about the brain exposure such compounds achieve. ADMET prediction separates the parent glycosides from their phenolic metabolites completely (Table 9, Figure 7): all three parent compounds fail Lipinski and Veber criteria and are predicted non-penetrant, driven by topological polar surface area of 190–212 Å², while both metabolites are predicted penetrant with the highest composite scores in the set. Tacrolimus is predicted non-penetrant, yet systemically administered FK506 reduces abnormal prion protein in brain and prolongs survival in prion-infected mice(Nakagaki et al., 2020; Nakagaki et al., 2013); predicted non-penetrance is therefore read as suggestive rather than decisive.

4. Dysregulated glucocorticoid signalling in sCJD in context

Three of the findings reported in Section 3 require a broader context to be considered in order to further their interpretation. Serum cortisol in sCJD is elevated by a median of 147.9 nM (Dabin et al., 2020), and FKBP5 is elevated in both compartments. The cortisol measurement carries its own caveats — 39 patients against 52 controls, samples drawn between 10:00 and 16:00 without standardisation to a fixed time of day — and we weight it accordingly. FKBP51 is a negative

regulator of the glucocorticoid receptor, and the canonical demonstration of that relationship is precisely this combination: New World primates maintain high circulating cortisol to compensate for low-affinity receptors, and elevated FKBP51 is the unequivocal cause, raising the dexamethasone EC50 roughly seventeen-fold when expressed heterologously (Denny et al., 2000). High cortisol together with high FKBP51 would be consistent with glucocorticoid resistance rather than with glucocorticoid excess, and on the reading we adopt sCJD presents both halves of that pattern. Because the source is internally inconsistent about the direction (Section 3.2), it is worth stating what turns on it. The compensatory reading, in which cortisol climbs because receptors are insensitive, is the one that needs elevation and the one the primate comparison supports. Were the legend correct and cortisol instead low, the inference would change character without reversing: low ligand alongside a receptor complex held in its low-affinity state would describe a host response with the same brake disengaged for a different reason, and would make a corticosteroid no more attractive. The claim that glucocorticoid signalling is impaired survives either reading; the particular mechanism by which it is impaired does not. A third possibility deserves mention, since it links this uncertainty to the confound of Section 6: exogenous glucocorticoids suppress endogenous cortisol, so steroid treatment in a subset of patients would depress the measured concentration while raising FKBP5, producing the legend's direction for a reason that is itself the confound. The inference no longer rests on those two measurements alone, which do derive from different studies of the disease rather than from the same individuals: Section 3.4 shows the chaperone complex itself shifted toward its FKBP51-bound, low-affinity configuration within the brain tissue, receptor transcript being unmeasurable on that platform.

That reframes the milieu of FtKBP5 as a target. In Section 3.7, we showed FKBP5 that unresponsive to prion protein abundance and Section 3.8 placed it within a host response shared with chronic CNS infection. Neither observation is a weakness once the disease is considered as the transmissible condition it is. Modulating the host response in CNS infection is an established and effective strategy: adjuvant dexamethasone in adults with bacterial meningitis reduced unfavourable outcomes (relative risk 0.59, 95% CI 0.37–0.94) and mortality (relative risk 0.48, 95% CI 0.24–0.96), with the largest effect in pneumococcal disease, where unfavourable outcomes fell from 52% to 26%(de Gans & van de Beek, 2002).

Corticosteroids would nevertheless not be a fruitful intervention in sCJD, and for a specific mechanistic reason. If FKBP5 is elevated, receptor sensitivity is reduced, so a steroid must overcome that resistance before it can act — and, as we report on Section 4.1, administering one deepens the resistance rather than overcoming it. FKBP51 inhibition addresses the resistance itself. Silencing FKBP51 produces a ten-fold increase in dexamethasone potency against IL-1β-induced IL-6 and IL-8, while overexpression reduces prednisolone sensitivity in vivo; immunoprecipitation places FKBP51 in a complex containing Hsp90, the glucocorticoid receptor and members of the IKK family, and silencing it independently reduces NF-κB p50/p65 nuclear translocation with downstream reductions in ICAM expression and cytokine secretion (Kästle et al., 2018). The authors propose FKBP51 inhibition as a means of controlling steroid-refractory inflammation in a steroid-dependent and steroid-independent manner simultaneously. This proposal may be worth examining in sCJD based on our own findings.

An integrative hypothesis may thus be stated as follows. sCJD involves a host response in which glucocorticoid signalling is dysregulated: the chaperone complex around the receptor is shifted toward its FKBP51-bound, low-affinity configuration, and the receptor’s canonical

transcriptional programme is not correspondingly engaged, so that the host-response programme characterised in Section 3.6 proceeds with its principal negative-feedback brake disengaged. Whether this reflects reduced receptor sensitivity in the presence of elevated cortisol, as the New World primate comparison would suggest, is a specific and testable reading of that state rather than a description of it. FKBP51 inhibition is predicted to act on both limbs — restoring receptor sensitivity and suppressing NF-κB directly — where corticosteroids would act on neither efficiently.

4.1 Further context from prion-specific studies

A proposal about host-response modulation in prion disease has to be tested against what is already known in prion disease itself. On the human side there is no trial or cohort study of corticosteroid treatment in pathologically confirmed Creutzfeldt–Jakob disease. Corticosteroids nevertheless reach these patients routinely, because an empirical steroid trial is standard in the workup of rapidly progressive dementia, where a response is taken to identify a treatable mimic(Hermann & Zerr, 2022) — most often steroid-responsive encephalopathy associated with autoimmune thyroiditis, which has a documented CJD-mimicking form, or another autoimmune encephalitis(Zhou et al., 2016). Exposure is therefore common: in the one series we identified that records it, available in abstract form, 23 of 64 patients with CJD had received glucocorticoids, with no detectable effect on survival(Sarandria, 2025).

Reports of harm rather than of benefit have, however, appeared, and the form that harm takes is informative. The same clinical practice has a bearing on our own brain data, since corticosteroids given before death would raise FKBP5 for reasons unrelated to the mechanism proposed here; that confound is set out in Section 6. In a patient with definite sporadic CJD and high anti-thyroid antibody titres, corticosteroid pulse therapy was followed by aggravation of seizure

activity, with generalised myoclonus, epilepsia partialis continua and ballistic dyskinesia(Jang et al., 2014). In a second patient, confirmed by RT-QuIC, a short course of glucocorticoid produced three days of apparent improvement followed by rapid deterioration within a week(Wu et al., 2025). A transient benefit that then extinguishes itself is a specific pattern rather than a general one, and it is the pattern this hypothesis predicts.

The explanation would appear to lie in the position FKBP5 occupies within steroid signalling, where it functions as a component of the control loop rather than as a bystander. FKBP5 transcription is induced by glucocorticoid receptor activation through intronic hormone response elements, and the FKBP51 protein that results lowers receptor affinity for cortisol and slows nuclear translocation — an ultra-short negative feedback loop on receptor sensitivity(Binder, 2009). Giving a corticosteroid to a patient whose FKBP5 is already elevated therefore does two things at once: it engages a receptor that is already desensitised, and it further induces the protein responsible for the desensitisation. A brief effect that extinguishes itself is the predicted consequence; one report describes exactly that course — an initial response followed by decline(Wu et al., 2025) — while the other describes symptomatic aggravation after pulse therapy without a benefit phase(Jang et al., 2014). The same loop yields a measurable prediction: blood FKBP5 should rise after steroid exposure in these patients. We are aware of no published measurement of blood FKBP5 expression or methylation in CJD patients exposed to corticosteroids; such a measurement would require only blood from patients already receiving an empirical steroid trial during diagnostic workup.

A second mechanism points in the same direction. Prolonged dexamethasone exposure drives primary microglia into a ramified but dysfunctional, senescence-like state with reduced phagocytosis, reduced cytokine production and reduced proliferation, and the change does not

reverse on washout(Borghammer & Van Den Berge, 2019). Read together with the depletion experiments described below, this is an unfavourable combination: the steroid suppresses the phagocytic function that protects against prions, while the anti-inflammatory signal for which it was given encounters a resistant receptor.

In animal models the evidence falls into three strands, and they do not all point the same way (Table 11). The oldest strand is about steroids directly: prednisone reduced susceptibility to scrapie in mice(Outram et al., 1974), and anti-inflammatory treatment prolonged incubation(Outram et al., 1975). Both effects were obtained with peripheral inoculation and act on lymphoreticular replication before neuroinvasion — a phase that no longer exists in a symptomatic patient. They support host-pathway modulation as a principle while saying little about the clinical setting.

The second strand bears more directly on the proposal, and the evidence in it is substantial. FKBP-binding pharmacology has already modified prion disease in vivo. FK506 reduced abnormal prion protein by activating autolysosomal degradation, attenuated microgliosis and prolonged survival when given from day 20 after inoculation(Nakagaki et al., 2013). Calcineurin inhibition begun at the clinical phase reduced neurodegeneration and extended survival while leaving PrP^{sc} accumulation unchanged, which shows that benefit in this disease need not run through prion clearance(Mukherjee et al., 2010). Most pertinently, oral FK506 in knock-in mice expressing chimeric human prion protein and inoculated with sCJD prions — not a mouse-adapted strain — suppressed gliosis and significantly, if modestly, prolonged survival whether started just before or just after onset, and the authors concluded that a clinical trial would be worthwhile(Nakagaki et al., 2020). In hamsters, FK506 combined with minocycline lowered GFAP and IBA-1, reduced IL-1β and TNF-α, blocked NF-κB nuclear translocation and raised

the NRF2–HO-1 axis(Shah et al., 2019): both arms characterised in Section 3.6, moved in the intended directions by an FKBP ligand.

This requires a reconsideration on how tacrolimus should be positioned relative to our proposal. FK506 is not a poor comparator to be set aside on the grounds that it is immunosuppressive; it is an FKBP ligand that modifies prion disease in vivo, including against human prions(Nakagaki et al., 2020; Nakagaki et al., 2013), although its benefit is usually attributed to downstream calcineurin inhibition rather than to FKBP engagement itself, including against human prions. Which member of the FKBP family carries the effect, however, remains unestablished. FK506 binds FKBP12 and inhibits calcineurin and does not selectively engage FKBP51, whereas SAFit2 engages FKBP51 selectively and is not immunosuppressive(Gaali et al., 2014). At least four mechanisms have been proposed for FK506 in this disease: calcineurin inhibition, induction of autophagy, reduced PrP^{c} expression through defective endoplasmic-reticulum translocation, and FKBP10-dependent effects on PrP^{c} biogenesis(Mukherjee et al., 2010; Nakagaki et al., 2013; Stocki et al., 2016). SAFit2 isolates one of them. The prediction is correspondingly sharp: if the benefit runs through FKBP51 and autophagic flux, SAFit2 should reproduce it without immunosuppression and without lowering PrP^{c}; whereas if it runs through calcineurin or through FKBP10-dependent PrP^{c} biogenesis, SAFit2 would be expected to fail in an experiment in which FK506 succeeds. We would note that the PRNP-depletion result of Section 3.7 was obtained in non-neural, uninfected cells, and does not by itself determine whether a SAFit2 benefit, were one observed, would act on the host response or on prion protein abundance. A head-to-head comparison with PrP^{c} measured as well as PrP^{sc} would separate these, and a negative result would be as informative as a positive one.

Host-response modulation strategies in sCJD may also carry significant risk, however, that requires consideration when designing such. Microglia are protective in prion infection. Ablating them aggravated prion neurotoxicity in organotypic slices and in vivo, and interleukin-34 deficiency accelerated disease with increased prion protein deposition(Zhu et al., 2016). Depleting 78–90% of cortical microglia with a CSF-1R inhibitor accelerated vacuolation, astrogliosis and PrP^{sc} deposition in RML scrapie, bringing euthanasia forward by 31 days when treatment began early after infection and by 33 days when it began at 80 days post-infection; clinical disease was accelerated with the ME7 and 22L strains as well, for which no survival figures are given(Carroll et al., 2018). In mice whose microglia fail to develop, disease was faster even though prion accumulation was lower, with earlier non-polarised reactive astrocytosis, which suggests that microglia restrain harmful astrocyte behaviour rather than simply clearing prions(Bradford et al., 2022).

The same compartment is nonetheless capable of harm, and it is the combination of the two properties that makes it an interesting target rather than a contradictory one. Microglia in prion-diseased brain carry little proinflammatory cytokine at baseline but are primed: a single systemic endotoxin challenge produces exaggerated IL-1β, TNF-α and IFN-β, acute cognitive and motor deterioration, increased neuronal apoptosis and earlier onset of disease-associated impairment, none of which occurs in challenged controls(Cunningham et al., 2009; Cunningham et al., 2005). A compartment that is necessary but primed to over-respond is precisely the phenotype that elevated FKBP51 against a background of elevated cortisol would be expected to produce: the cells are intact and functioning, but the brake upon them is disengaged.

We regard this as a substantive limitation of host-response modulation approaches in sCJD therapeutics, but one that accentuates their potential positioning. Currently, these assorted

experiments deplete microglia; our suggestion based on this analysis is to restore is a canonical function, i.e. a negative-feedback loop operating within them, and the distinction is not merely a verbal one. Corticosteroids render microglia ramified and functionally impaired(Park et al., 2019) while CSF1R blockade depletes them outright(Bradford et al., 2022; Carroll et al., 2018); both therefore perturb a compartment these experiments show to be host-protective, and a corticosteroid additionally fails on the second count by deepening the resistance it was given to overcome. FKBP51 inhibition lowers the set-point of that resistance instead, re-sensitising the brake to the cortisol the patient already has, without depleting microglia or blocking phagocytosis — and the FK506 studies above extended survival while attenuating microgliosis rather than abolishing it. The risk is nonetheless real, and it sets a requirement rather than a caveat: in any trial of SAFit2 in a prion model, microglial number and phagocytic capacity must be measured and not assumed, and survival, in place of gliosis score, must be the primary endpoint. A compound that improved histological gliosis while shortening survival would otherwise appear successful on the wrong endpoint.

The strength of the human evidence should not be overstated, and its limits are set out here rather than left to inference. The reports of worsening are two cases. The single series that records steroid exposure found no survival difference and is available only as an abstract. Confounding by indication is unavoidable, since steroids are given when the diagnosis is uncertain and the patient is deteriorating, and deterioration is the natural history of the disease. The induction mechanism is inferred from non-prion systems and has never been measured before and after steroid exposure in a patient with CJD. Taken together, this evidence indicates that corticosteroids are an implausible route to modulating this host response and may aggravate it. It does not support the stronger claim that they shorten survival, and we do not make that claim.

4.2 FKBP5 as a target in sCJD and its implications

Prion disease has one accepted genetic modifier and no molecular stratifier. PRNP codon 129 strongly influences duration and subtype yet has not accounted for variation across brain transcriptome, blood miRNA or blood methylation. For trial design in a rapidly progressive disease with wide survival variation, that gap is significant.

FKBP5 is among the best-characterised pharmacogenetic loci in medicine. Common haplotypes indexed by rs1360780 alter receptor sensitivity and the magnitude of FKBP51 induction, and genotype at that locus predicts response to standardised versus naturalistic antidepressant treatment, with a significant genotype-by-treatment-mode interaction(Stamm et al., 2015). A target whose variants are already known to modify response to drugs acting on the same axis is a different proposition from one identified by expression alone. One apparent caveat should be named: the largest post-mortem study of FKBP5 in human cortex found effects of psychopathology and of age on expression but none of genotype(Matosin et al., 2023). This remains compatible with the pharmacogenetic proposal, since the genotype effect concerns the magnitude of induction following receptor activation rather than baseline abundance(Binder, 2009) — but it does mean genotype cannot be read off expression, and a trial would have to genotype directly. The same locus governs the hazard described in Section 4.1: rs1360780 genotype sets the magnitude of FKBP5 induction following receptor activation(Binder, 2009), so it predicts not only response to agents acting on this axis but also which patients a corticosteroid would desensitise most deeply.

A candidate pharmacodynamic readout is moreover available, although the evidence supporting it concerns diagnostic and prognostic association rather than demonstrated response to treatment. FKBP5 methylation sits within the replicated four-locus blood signature; AIM2 methylation in

the same panel tracks decline on the MRC Prion Disease Rating Scale; and methylation at three of the 38 significant sites associates with 97 days of additional median survival independently of codon 129(Dabin et al., 2020). A trial of an FKBP51-directed agent could stratify on genotype and follow response on an existing blood panel, which is normally the hardest element to assemble in this disease.

4.3 Anthocyanins as complementary repurposing candidates in sCJD

Anthocyanins act on propagation — Keap1–NRF2 engagement, PrP^{sc} clearance and complete inhibition of real-time quaking-induced conversion seeded with CJD cerebrospinal fluid(Christoudia et al., 2024) — whereas FKBP51 inhibition acts on the host response. These are complementary limbs of the same disease process rather than competing nominations, and the ADMET result in Section 3.10 indicates that the propagation arm requires a brain-penetrant species, directing attention to the metabolites rather than the parent glycosides.

The proposed utilization of anthocyanins however comes with several limitations. Specifically, no genotype data were analysed here; the pharmacogenetic proposal is prospectively testable, not established. The meningitis evidence is pathogen- and setting-dependent, strongest for pneumococcal disease in high-income settings, and is cited as precedent for host-response modulation in CNS infection rather than as a direct therapeutic analogy. And we do not demonstrate glucocorticoid resistance in the formal sense: the dissociation reported here is between transcript layers, and reduced receptor sensitivity would have to be shown by a receptor-sensitivity assay in sCJD patients — which is itself a tractable experiment.

5. Discussion

Cross-compartment integration of the public sCJD data has been attempted and returned no shared gene(Oberoi et al., 2026). The analyses presented herein substitute a narrower question for that one, asking of each locus with replicated evidence in the periphery whether it also carries evidence in brain, and they return a single gene. What follows considers the pharmacology available against that gene, the relation of the present reading to work already published on it, and the experiment that would test the proposal.

SAFit2 achieves selectivity for FKBP51 over the near-identical FKBP52 by an induced-fit mechanism(Gaali et al., 2014) and is the established chemical probe for this pharmacology(Buffa et al., 2023). It has reduced pathology in three separate protein-misfolding diseases: tau oligomer burden in PS19 mice with demonstrated brain penetrance over a 28-day regimen(Contreras-Marciales et al., 2026); ubiquitin-positive inclusions with preserved nigral neurons and improved motor function in a neuromelanin–α-synuclein model(Garcia-Gomara et al., 2025); and mutant huntingtin through mTOR-independent autophagic flux(Bailus et al., 2021). It additionally suppresses NF-κB while restoring mitochondrial function(Ji et al., 2026), which addresses the inflammatory arm characterised here. Nor is it immunosuppressive, a consideration of some weight in a disease where the innate immune compartment is host-protective (Section 4.1).

The novelty of this work requires precise statement. A PubMed search for FKBP5 or FKBP51 together with prion disease returns three records: the methylation study(Dabin et al., 2020), the network analysis that lists FKBP5 among ten hubs without pursuing it(Mredul et al., 2022), and one match arising from an institutional name and not from content(Matosin et al., 2023). Of these, only the methylation study pursued FKBP5 directly, measuring serum cortisol in response to the FKBP5 finding, proposing the hypothalamic-pituitary-adrenal axis as a candidate link between brain pathology and the periphery, and assembling the existing FK506 literature in prion

models in support. The present work builds directly on that reading rather than claiming it was overlooked.

It should be noted that FKBP-directed pharmacology new to this disease. Beyond the FK506 studies reported on Section 4.1, inhibition of the FKBP family causes abortive translocation of PrP^{c} into the endoplasmic reticulum with subsequent proteasomal degradation, and depletion of the ER-luminal member FKBP10 reproduced much of that effect and reduced PrP^{sc} propagation in cell models, leading its authors to nominate FKBP10 as a therapeutic target(Stocki et al., 2016). No study to date, however, has tested a selective FKBP51 inhibitor in any prion model, proposed FKBP51 as the relevant member of the family, or interpreted the sCJD phenotype as dysregulated glucocorticoid signalling rather than as hypothalamic-pituitary-adrenal activation.

The experiment that would test this proposal is straightforward to specify: SAFit2 in a chronically prion-infected cell line and in RML- or ME7-infected mice, with survival as the primary endpoint and PrP^{sc} load, LC3-II and autophagic flux, NF-κB target expression and gliosis alongside it, plus real-time quaking-induced conversion seeded with patient cerebrospinal fluid as a cell-free arm. Section 4.1 dictates two features of the design. An FK506 comparator arm is needed, because FK506 already works in this setting and the question is whether FKBP51 is what carries it; and microglial number and phagocytic capacity must be measured rather than assumed, because depleting that compartment accelerates prion disease. Those endpoints discriminate mechanism instead of merely registering an effect: PrP^{tc} falling with LC3-II rising implicates the proteostatic arm, whereas gliosis and NF-κB targets falling without it implicates the inflammatory arm. The result of Section 3.7 would predict that any benefit acts on the host response rather than on prion protein abundance, and that discrimination is testable within the same experiment.

6. Context, strengths and limitations

This work sits alongside two prior integrative analyses of the same material. Oberoi and colleagues established the cross-layer no-overlap result that frames the question(Oberoi et al., 2026), and Mredul and colleagues combined the two brain series into a protein-interaction network, nominating ten hub proteins including FKBP5 and CDKN1A without following either further(Mredul et al., 2022); a further integrative analysis nominated hub genes and candidate agents from overlapping material(Cheng et al., 2023). Our contribution is to reanalyse the underlying data instead of aggregating published signatures, to establish systematically what data exist, and to ask the single-gene cross-compartment question that the signature-overlap framing cannot address.

Several aspects of the present work may be counted among its strengths. The dataset survey is systematic and reproducible, using seven independent query formulations with documented screening (Table 1), which identified six series not considered by prior work. All reanalysis was performed from source, not from published signatures, which surfaced a silent contrast-direction inversion that produces a complete and plausible-looking result table with every sign reversed. The central replication is cross-platform and cross-laboratory, with bootstrap and leave-one-out stability reported in place of a single point estimate. And the cell-composition question was addressed by direct test, genome-wide and against a matched peer set, instead of being acknowledged as a caveat. Working from the raw intensity file also allowed one of our own earlier results — a reported difference in scaling between the antioxidant and inflammatory arms — to be checked and withdrawn (Section 3.6).

Our work should be interpreted within its context and limitations. It is computational throughout and generates no new experimental observation; every mechanistic edge connecting FKBP51 to

autophagic clearance derives from tau, α-synuclein or huntingtin models, and whether those edges hold in prion disease is the hypothesis under test rather than a premise of it.

Bulk post-mortem cortex confounds per-cell regulation with cellular composition. After adjustment no gene set retains a group effect, so the pathway-level findings describe a programme proportionate to glial burden and do not establish per-cell induction. The same confound applies to FKBP5, which tracks the microglial score at r = 0.839. It retains a composition-independent component where the gliosis markers do not (Section 3.3), although that analysis is underpowered at the available sample size, and we would therefore put the claim no higher than the data allow: among loci carrying replicated peripheral epigenetic evidence together with independent brain-network evidence, FKBP5 is the one that is also elevated in brain, pharmacogenetically characterised and addressable by a selective brain-penetrant inhibitor. Whether it is the most elevated or the most specific gene in sCJD cortex is a question these data cannot settle against the wider glial programme, and one we do not raise.

The most serious of these limitations is one our own argument makes likely, and the deposited data cannot address. FKBP5 is the canonical glucocorticoid-responsive gene: its transcription is driven directly by the activated receptor through intronic hormone response elements, which is the very property Section 4 relies on. Corticosteroids are given to a proportion of patients who prove to have sCJD, usually while an autoimmune encephalopathy is still under consideration, and the case literature on that practice is cited here in support of a different point. Premortem corticosteroid exposure in even a minority of the eleven cases would therefore raise FKBP5 in cortex for a reason that has nothing to do with the mechanism proposed. Agonal stress, terminal hypoxia, prolonged intensive care and the cortisol rise accompanying any protracted terminal illness would act in the same direction. The deposited GSE124571 matrix carries sample

identifiers alone, with no age, sex, post-mortem interval, agonal state, cause of death or drug exposure, so none of this can be adjusted for or even described. The published kinetics of FKBP5 induction bound this confound more usefully than any of our own observations, and we set them out because they narrow it without dissolving it. In vivo, a single dose of dexamethasone at 10 mg/kg raises Fkbp5 mRNA in mouse brain within one to four hours, peaks it at four to eight, and leaves it indistinguishable from baseline by 24 hours in every region tested — 105% of vehicle in the central amygdala, 98% in the paraventricular nucleus, 85% in CA1, with the dentate gyrus undershooting to 73%(Scharf et al., 2011). The same study notes that this differs from lymphoblast culture, where elevation persists at 24 hours(Vermeer et al., 2003), and attributes the difference to the limits of in vitro kinetics. Because the empirical steroid trial in rapidly progressive dementia is typically given during the diagnostic phase, weeks to months before death in a disease whose median survival is measured in months, a single pulse course falls well outside that window and is an improbable explanation for a transcript difference measured at autopsy.

Two exposures nonetheless remain inside it. Sustained administration behaves differently from a single dose: four weeks of corticosterone raises Fkbp5 in hippocampus, hypothalamus and blood, and lowers its DNA methylation in each(Lee et al., 2010). That matters significantly, because it is also the most parsimonious alternative account of the peripheral finding this paper is built on — chronic glucocorticoid exposure produces FKBP5 hypomethylation in blood, which is precisely the replicated mark reported in sCJD. And the agonal window is squarely inside the induction window: a terminal cortisol surge in the final hours of life would raise FKBP5 in cortex by exactly the mechanism described. What would settle the question is drug-exposure data, or measurement in a series where steroid administration is documented; these however

were also unaccounted for in the original investigations. We would urge that any prospective test record it.

Three further constraints follow from the platform rather than from the biology. Sex cannot be verified in GSE124571: of the sex-informative transcripts only DDX3Y is carried on this array, and it sits at background in all 21 samples, so the sex argument of Section 3.5 rests on GSE160208 alone. The dominant axis of variation accounts for 54.5% of the variance, separates the two groups ($p = 0.0010$) and correlates with array median intensity ($r = -0.53$) and with array dynamic range ($r = +0.49$). Array median intensity does not differ between groups ($p = 0.43$), but array dynamic range does ($p = 0.041$), so at 21 arrays a partly technical contribution to the group separation cannot be excluded. And the identity of the technical replicate is taken from the series metadata rather than recovered from the matrix: two array pairs are tied at $r = 0.996$, so the donor-level analysis of Section 2.4 assumes a pairing it cannot independently confirm.

Throughout, transcript abundance is relied upon as a proxy for protein, and the appropriateness of that proxy is uneven across the claims made. It is weakest for the chaperone complex of Section 3.4, where the quantity of interest is the composition of an assembled Hsp90-receptor complex rather than a ratio of transcripts; establishing that composition would require co-immunoprecipitation from the same tissue, and our data indicate only that the relative availability of the two co-chaperones has shifted. The proxy is firmer for FKBP5 itself, for which transcript and protein have been shown to move together in human cortex across disease state and age by immunoblot and immunohistochemistry alongside several RNA methods (Matosin et al., 2023).

Whether the FKBP5 signal is glial or neuronal remains unresolved. The public single-nuclei data lack the depth and the glial representation required to settle it (Section 3.9), and purpose-generated data rather than further reanalysis will be needed.

Two further limitations concern mechanism rather than these data. Microglia are host-protective in prion models, so any intervention reaching the innate immune compartment carries a risk of harm, and our argument that re-sensitising glucocorticoid signalling differs from suppressing or depleting that compartment (Section 4.1) is reasoning and not a result. Age is an unmeasured confounder: FKBP5 rises with age in human cortex, neither brain series reports donor age in a form permitting adjustment, and an age contribution to the group difference therefore cannot be excluded. Finally, the pharmacogenetic proposal of Section 4.2 is a hypothesis; no genotype data accompanied any of the series reanalysed here.

Th. GSE156994 was not reanalysed because GEO distributes only raw intensity files for it, and the published differentially methylated positions are already composition-corrected and replicated in an independent cohort of 186 individuals. Furthermore, the blood miRNA layer is cited from its original qPCR replication and not from the public abundance matrix, which is dominated by a single species accounting for 79–86% of reads and shows group-confounded library complexity; under median-of-ratios normalisation the reported miRNAs fall at the centre of the distribution (**Figure 5**), so that matrix cannot establish specificity. The authors' independent qPCR replication is what carries that layer, and our analysis clarifies why it was necessary.

7. Conclusions

Four public sCJD datasets share no common gene network, a result that the present work does not overturn. They nevertheless converge on a single gene. FKBP5 carries a replicated peripheral epigenetic mark, a position as a hub in an independent brain network analysis, and transcript elevation in two independent brain cohorts across both sampled regions that is not explained by

sex. Published mechanism places the inflammatory, oxidative and proteostatic processes of this disease downstream of it, while its indifference to prion protein abundance places it in the host response rather than in prion biology. It is also, and separately, a pharmacogenetically characterised locus(Stamm et al., 2015) and the target of SAFit2, a selective FKBP51 antagonist(Gaali et al., 2014) that is active in the central nervous system after peripheral administration(Hartmann et al., 2015), an inhibitor that has reduced aggregate burden in three other protein-misfolding diseases and has never been tested against prions. That experiment, with stratification and pharmacodynamic readouts already available, is the most informative next step these data support.

Author contributions

G.V.: conceptualisation, methodology, formal analysis, investigation, data curation, software, visualisation, writing — original draft, writing — review and editing, supervision. [Co-author 2]: [CRediT roles]. All authors read and approved the final manuscript and accept responsibility for its contents. Contributions are described using the CRediT taxonomy.

Declaration of generative AI and AI-assisted technologies

During the preparation of this work the authors used Claude (Anthropic) for the following tasks: reanalysis of GSE124571 from the raw intensity file; implementation and documentation of the analysis script distributed as Supplementary Software; the systematic survey of candidate datasets reported in Table 1; the literature searches underlying Sections 4.1 and 5; and drafting of the manuscript text. The authors verified the computational results against independently processed values for the same series, reviewed and edited all text, and take full responsibility for the content of this publication. Twenty-eight load-bearing citations were checked against their sources, nineteen of them at the level of the abstract or record rather than the full text and one,

for which no copy was retrievable, not at all; the outcome of that audit, including six citations found to be only partly accurate, is reported in the Appendix. In accordance with the positions of the International Committee of Medical Journal Editors and the Committee on Publication Ethics, the tool is not listed as an author, since it cannot take responsibility for the work or declare competing interests.

Funding

[Funding statement. If the work received no specific grant, state: This research received no specific grant from any funding agency in the public, commercial or not-for-profit sectors.]

Data availability

This study generated no new primary data. Every dataset analysed is publicly archived in the NCBI Gene Expression Omnibus and was obtained from there without restriction: GSE124571 and GSE160208 (sCJD brain transcriptome), GSE140069 (blood miRNA), GSE156994 (blood methylation, used as published because the archive carries only raw IDAT files for that series), GSE330903 (PRNP depletion) and GSE35864 (HIV brain severity series). The ten series considered at screening, with the reason each was retained or excluded, are listed in Table 1. The analysis code that reproduces every GSE124571 figure reported here, together with the derived result tables S1 to S4, a provenance record and the adversarial checks of Sections 2.3, 3.4 and 6, is distributed as Supplementary Software and is archived at [repository DOI, to be minted on acceptance]. Running it requires the deposited GSE124571 non-normalised intensity file, which the script locates by its archive filename.

Competing interests

The authors declare no competing interests. No author has a financial relationship with any entity developing FKBP51-directed compounds.

Ethics

This study is a secondary analysis of de-identified, publicly archived datasets and required no additional ethical approval. Ethical approvals for the primary studies are reported in their original publications.

References

Areškevičiūtė, A., High, H., Broholm, H., & Lund, E. L. (2021). Regional Differences in Neuroinflammation-Associated Gene Expression in the Brain of Sporadic Creutzfeldt-Jakob Disease Patients. *International Journal of Molecular Sciences*, *22*(1), 140.

Bailus, B. J., Scheeler, S. M., Simons, J., Sanchez, M. A., Hausch, F., Kennedy, B. K., Ehrlich, M. E., & Ellerby, L. M. (2021). Modulating FKBP5/FKBP51 and autophagy lowers HTT (huntingtin) levels. *Autophagy*, *17*(12), 4119–4140. https://doi.org/10.1080/15548627.2021.1904489

Barrett, T., Wilhite, S. E., Ledoux, P., Evangelista, C., & Soboleva, A. (2013). NCBI GEO: archive for functional genomics data sets - update. *Nucleic Acids Research*, *41*, D991–D995. https://doi.org/10.1093/nar/gks1193

Bartoletti-Stella, A., Baiardi, S., Stanzani-Maserati, M., Parchi, P., & Capellari, S. (2019). Analysis of RNA expression profiles identifies dysregulated vesicle trafficking pathways in Creutzfeldt-Jakob disease. *Molecular Neurobiology*, *56*(7), 5009–5024.

Benjamini, Y., & Hochberg, Y. (1995). Controlling the false discovery rate: a practical and powerful approach to multiple testing. *Journal of the Royal Statistical Society Series B*, *57*(1), 289–300.

Binder, E. B. (2009). The role of FKBP5, a co-chaperone of the glucocorticoid receptor in the pathogenesis and therapy of affective and anxiety disorders. *Psychoneuroendocrinology*, *34 Suppl 1*, S186–S195. https://doi.org/10.1016/j.psyneuen.2009.05.021

Borghammer, P., & Van Den Berge, N. (2019). Brain-First versus Gut-First Parkinson's Disease: A Hypothesis. *J Parkinsons Dis*, *9*(s2), S281–s295. https://doi.org/10.3233/jpd-191721

Bradford, B. M., McGuire, L. I., Hume, D. A., Pridans, C., & Mabbott, N. A. (2022). Microglia deficiency accelerates prion disease but does not enhance prion accumulation in the brain. *Glia*, *70*(11), 2169–2187. https://doi.org/10.1002/glia.24244

Buffa, V., Knaup, F. H., Heymann, T., Springer, M., Schmidt, M. V., & Hausch, F. (2023). Analysis of the Selective Antagonist SAFit2 as a Chemical Probe for the FK506-Binding Protein 51. *ACS Pharmacology and Translational Science*, *6*(3), 361–371. https://doi.org/10.1021/acsptsci.2c00234

Carroll, J. A., Race, B., Williams, K., Striebel, J., & Chesebro, B. (2018). Microglia are critical in host defense against prion disease. *Journal of Virology*, *92*(15), e00549–00518. https://doi.org/10.1128/JVI.00549-18

Cheng, J., Chen, L., & Hu, Z. (2023). Identification of hub genes and therapeutic agents for sporadic Creutzfeldt-Jakob disease by integrated bioinformatics analysis. *Scientific Reports*, *13*, 14122.

Christoudia, N., Xanthopoulos, K., & Sklaviadis, T. (2024). Anthocyanins activate the Keap1-NRF2 pathway and reduce prion propagation. *Redox Biology*, *72*, 103133.

Contreras-Marciales, A., Mezquite-Garcia, D., Verdina, L. A., Hill, S. E., & Blair, L. J. (2026). FKBP51 inhibition by SAFit2 modulates tau pathology and cognitive deficits in PS19 mice. *Alzheimer's Research and Therapy*, *18*(1). https://doi.org/10.1186/s13195-026-02107-3

Cunningham, C., Campion, S., Lunnon, K., Murray, C. L., Woods, J. F. C., Deacon, R. M. J., Rawlins, J. N. P., & Perry, V. H. (2009). Systemic inflammation induces acute behavioral

and cognitive changes and accelerates neurodegenerative disease. *Biological Psychiatry*, *65*(4), 304–312. https://doi.org/10.1016/j.biopsych.2008.07.024

Cunningham, C., Wilcockson, D. C., Campion, S., Lunnon, K., & Perry, V. H. (2005). Central and systemic endotoxin challenges exacerbate the local inflammatory response and increase neuronal death during chronic neurodegeneration. *Journal of Neuroscience*, *25*(40), 9275–9284. https://doi.org/10.1523/JNEUROSCI.2614-05.2005

Dabin, L. C., Guntoro, F., Campbell, T., Bélicard, T., Smith, A. R., Smith, R. G., Raybould, R., Schott, J. M., Lunnon, K., Sarkies, P., Collinge, J., Mead, S., & Viré, E. (2020). Altered DNA methylation profiles in blood from patients with sporadic Creutzfeldt-Jakob disease. *Acta Neuropathologica*, *140*(6), 863–879. https://doi.org/10.1007/s00401-020-02224-9

Davies, T. H., Ning, Y.-M., & Sánchez, E. R. (2002). A new first step in activation of steroid receptors: hormone-induced switching of FKBP51 and FKBP52 immunophilins. *Journal of Biological Chemistry*, *277*(7), 4597–4600. https://doi.org/10.1074/jbc.C100531200

de Gans, J., & van de Beek, D. (2002). Dexamethasone in adults with bacterial meningitis. *New England Journal of Medicine*, *347*(20), 1549–1556. https://doi.org/10.1056/NEJMoa021334

Denny, W. B., Valentine, D. L., Reynolds, P. D., Smith, D. F., & Scammell, J. G. (2000). Squirrel monkey immunophilin FKBP51 is a potent inhibitor of glucocorticoid receptor binding. *Endocrinology*, *141*(11), 4107–4113. https://doi.org/10.1210/endo.141.11.7785

Gaali, S., Kirschner, A., Cuboni, S., Hartmann, J., Bracher, A., & Hausch, F. (2014). Selective inhibitors of the FK506-binding protein 51 by induced fit. *Nature Chemical Biology*, *11*(1), 33–37. https://doi.org/10.1038/nchembio.1699

Garcia-Gomara, M., Legarra-Marcos, N., Serena, M., Cuadrado-Tejedor, M., & Garcia-Osta, A. (2025). FKBP51 inhibition ameliorates neurodegeneration and motor dysfunction in the neuromelanin-SNCA mouse model of Parkinson's disease. *Molecular Therapy*, *33*(3), 895–916. https://doi.org/10.1016/j.ymthe.2025.01.049

Gelman, B. B., Chen, T., Lisinicchia, J. G., & Morgello, S. (2012). The National NeuroAIDS Tissue Consortium brain gene array: two types of HIV-associated neurocognitive impairment. *PLoS One*, *7*(9), e46178. https://doi.org/10.1371/journal.pone.0046178

Hartmann, J., Wagner, K. V., Gaali, S., Kirschner, A., Kozany, C., Rühter, G., Dedic, N., Häusl, A. S., Hoeijmakers, L., Westerholz, S., Namendorf, C., Gerlach, T., Uhr, M., Chen, A., Deussing, J. M., Holsboer, F., Hausch, F., & Schmidt, M. V. (2015). Pharmacological Inhibition of the Psychiatric Risk Factor FKBP51 Has Anxiolytic Properties. *J Neurosci*, *35*(24), 9007–9016. https://doi.org/10.1523/JNEUROSCI.4024-14.2015

Hermann, P., & Zerr, I. (2022). Rapidly progressive dementias - aetiologies, diagnosis and management. *Nature Reviews Neurology*, *18*(6), 363–376. https://doi.org/10.1038/s41582-022-00659-0

Houseman, E. A., Accomando, W. P., Koestler, D. C., Christensen, B. C., Marsit, C. J., Nelson, H. H., Wiencke, J. K., & Kelsey, K. T. (2012). DNA methylation arrays as surrogate measures of cell mixture distribution. *BMC Bioinformatics*, *13*, 86. https://doi.org/10.1186/1471-2105-13-86

Jang, J.-W., Park, S. Y., Park, Y. H., Kim, J. E., & Kim, S. (2014). Symptomatic aggravation after corticosteroid pulse therapy in definite sporadic Creutzfeldt-Jakob disease with the feature of Hashimoto's encephalopathy. *BMC Neurology*, *14*, 179. https://doi.org/10.1186/s12883-014-0179-y

Ji, Y., Chen, W., Yao, L., Liu, F., Sun, X., & Wang, Z. (2026). FKBP51 mediates mitochondrial function via NF-κB pathway during sleep fragmentation-induced cognitive impairment. *Brain, Behavior, and Immunity*, *136*, 106556. https://doi.org/10.1016/j.bbi.2026.106556

Kästle, M., Kistler, B., Lamla, T., Bretschneider, T., Lamb, D., Nicklin, P., & Wyatt, D. (2018). FKBP51 modulates steroid sensitivity and NFκB signalling: A novel anti-inflammatory drug target. *European Journal of Immunology*, *48*(11), 1904–1914. https://doi.org/10.1002/eji.201847699

Lee, R. S., Tamashiro, K. L. K., Yang, X., Purcell, R. H., Harvey, A., Willour, V. L., Huo, Y., Rongione, M., Wand, G. S., & Potash, J. B. (2010). Chronic corticosterone exposure increases expression and decreases deoxyribonucleic acid methylation of Fkbp5 in mice. *Endocrinology*, *151*(9), 4332–4343. https://doi.org/10.1210/en.2010-0225

Matosin, N., Arloth, J., Czamara, D., & Binder, E. B. (2023). Associations of psychiatric disease and ageing with FKBP5 expression converge on superficial layer neurons of the neocortex. *Acta Neuropathologica*, *145*(4), 439–459. https://doi.org/10.1007/s00401-023-02541-9

Mredul, M. B. R., Khan, U., Rana, H. K., Meem, T. M., Awal, M. A., Rahman, M. H., & Khan, M. S. (2022). Bioinformatics and System Biology Techniques to Determine Biomolecular Signatures and Pathways of Prion Disorder. *Bioinformatics and Biology Insights*, *16*, 11779322221145373. https://doi.org/10.1177/11779322221145373

Mukherjee, A., Morales-Scheihing, D., Gonzalez-Romero, D., Green, K., Taglialatela, G., & Soto, C. (2010). Calcineurin inhibition at the clinical phase of prion disease reduces neurodegeneration, improves behavioral alterations and increases animal survival. *PLoS Pathogens*, *6*(10), e1001138. https://doi.org/10.1371/journal.ppat.1001138

Nakagaki, T., Ishibashi, D., Mori, T., Miyazaki, Y., Takatsuki, H., Tange, H., Taguchi, Y., Satoh, K., Atarashi, R., & Nishida, N. (2020). Administration of FK506 from late stage of disease prolongs survival of human prion-inoculated mice. *Neurotherapeutics*, *17*(4), 1850–1860. https://doi.org/10.1007/s13311-020-00870-1

Nakagaki, T., Satoh, K., Ishibashi, D., Fuse, T., Sano, K., Kamatari, Y. O., Kuwata, K., Shigematsu, K., Iwamaru, Y., Takenouchi, T., Kitani, H., Nishida, N., & Atarashi, R. (2013). FK506 reduces abnormal prion protein through the activation of autolysosomal degradation and prolongs survival in prion-infected mice. *Autophagy*, *9*(9), 1386–1394. https://doi.org/10.4161/auto.25381

Norsworthy, P. J., Thompson, A. G. B., Mok, T. H., Guntoro, F., Dabin, L. C., Nihat, A., Paterson, R. W., Schott, J. M., Collinge, J., Mead, S., & Viré, E. (2020). A blood miRNA signature associates with sporadic Creutzfeldt-Jakob disease diagnosis. *Nature Communications*, *11*(1), 3960. https://doi.org/10.1038/s41467-020-17655-x

Oberoi, M., Gurung, R., & Harris, D. A. (2026). Cross-omic analysis of sporadic Creutzfeldt-Jakob disease datasets. *International Journal of Molecular Sciences*, *27*, 6560.

Outram, G. W., Dickinson, A. G., & Fraser, H. (1974). Reduced susceptibility to scrapie in mice after steroid administration. *Nature*, *249*(460), 855–856. https://doi.org/10.1038/249855a0

Outram, G. W., Dickinson, A. G., & Fraser, H. (1975). Slow encephalopathies, inflammatory responses and arachis oil. *Lancet*, *1*(7900), 198–200. https://doi.org/10.1016/s0140-6736(75)91363-x

Park, M.-J., Park, H.-S., You, M.-J., Yoo, J., Kim, S. H., & Kwon, M.-S. (2019). Dexamethasone induces a specific form of ramified dysfunctional microglia. *Molecular Neurobiology*, *56*(2), 1421–1436. https://doi.org/10.1007/s12035-018-1156-z

Ratajczak, T., Ward, B. K., & Minchin, R. F. (2003). Immunophilin chaperones in steroid receptor signalling. *Current Topics in Medicinal Chemistry*, *3*(12), 1348–1357. https://doi.org/10.2174/1568026033451934

Ritchie, M. E., Phipson, B., Wu, D., Hu, Y., Law, C. W., Shi, W., & Smyth, G. K. (2015). limma powers differential expression analyses for RNA-sequencing and microarray studies. *Nucleic Acids Research*, *43*(7), e47. https://doi.org/10.1093/nar/gkv007

Sakamoto, Y., Makuuchi, M., Harihara, Y., Imamura, H., & Sato, H. (2000). Correlation between neurotoxic events and intracerebral concentration of tacrolimus in rats. *Biol Pharm Bull*, *23*(8), 1008–1010. https://doi.org/10.1248/bpb.23.1008

Sarandria, M. (2025). Dementia care research and psychosocial factors [conference abstract: Creutzfeldt-Jakob disease case series, treatment and survival].

Scharf, S. H., Liebl, C., Binder, E. B., Schmidt, M. V., & Müller, M. B. (2011). Expression and regulation of the Fkbp5 gene in the adult mouse brain. *PLoS One*, *6*(2), e16883. https://doi.org/10.1371/journal.pone.0016883

Shah, S. Z. A., Zhao, D., Taglialatela, G., Hussain, T., Dong, H., Sabir, N., Zhou, X., & Yang, L. (2019). Combinatory FK506 and minocycline treatment alleviates prion-induced neurodegenerative events via caspase-mediated MAPK-NRF2 pathway. *International Journal of Molecular Sciences*, *20*(5), 1144. https://doi.org/10.3390/ijms20051144

Smyth, G. K. (2004). Linear models and empirical Bayes methods for assessing differential expression in microarray experiments. *Statistical Applications in Genetics and Molecular Biology*, *3*(1), Article3. https://doi.org/10.2202/1544-6115.1027

Stamm, T. J., Rampp, C., Wiethoff, K., Stingl, J., Bauer, M., & Adli, M. (2015). The FKBP5 polymorphism rs1360780 influences the effect of an algorithm-based antidepressant treatment and is associated with remission in patients with major depression. *Journal of Psychopharmacology*, *30*(1), 40–47. https://doi.org/10.1177/0269881115620459

Stocki, P., Sawicki, M., Mays, C. E., Hong, S. J., Chapman, D. C., Westaway, D., & Williams, D. B. (2016). Inhibition of the FKBP family of peptidyl prolyl isomerases induces abortive translocation and degradation of the cellular prion protein. *Molecular Biology of the Cell*, *27*(5), 757–767. https://doi.org/10.1091/mbc.E15-10-0729

Vavougios, G. D. (2020). SARS-CoV-2 dysregulation of PTBP1 and YWHAE/Z gene expression: A primer of neurodegeneration. *Med Hypotheses*, *144*, 110212. https://doi.org/10.1016/j.mehy.2020.110212

Vavougios, G. D., Nday, C., Pelidou, S. H., Zarogiannis, S. G., Gourgoulianis, K. I., Stamoulis, G., & Doskas, T. (2020). Double hit viral parasitism, polymicrobial CNS residency and perturbed proteostasis in Alzheimer's disease: A data driven, in silico analysis of gene expression data. *Mol Immunol*, *127*, 124–135. https://doi.org/10.1016/j.molimm.2020.08.021

Vermeer, H., Hendriks-Stegeman, B. I., van der Burg, B., van Buul-Offers, S. C., & Jansen, M. (2003). Glucocorticoid-induced increase in lymphocytic FKBP51 messenger ribonucleic acid expression: a potential marker for glucocorticoid sensitivity, potency, and bioavailability. *Journal of Clinical Endocrinology and Metabolism*, *88*(1), 277–284. https://doi.org/10.1210/jc.2002-020354

Wei, Y., Li, S., Li, Z., Wan, Z., & Lin, J. (2022). Interpretable-ADMET: a web service for ADMET prediction and optimization based on deep neural representation. *Bioinformatics*, *38*(10), 2863–2871. https://doi.org/10.1093/bioinformatics/btac192

Wu, T.-C., Zhao, F., Liang, Y., Wu, Z.-Z., Chen, J.-B., Zhang, Z.-N., & Yang, H. (2025). Creutzfeldt-Jakob disease mimicking Hashimoto's encephalopathy: steroid response followed by decline. *Open Life Sciences*, *20*(1), 20251245. https://doi.org/10.1515/biol-2025-1245

Zayed, M., Tayara, H., & Jeong, B.-H. (2026). Ferroptosis-related mechanisms in prion diseases provide insights into neurodegeneration and reveal therapeutic implications. *Redox Biology*, *93*, 104155. https://doi.org/10.1016/j.redox.2026.104155

Zhou, J. Y., Xu, B., Lopes, J., Blamoun, J., & Li, L. (2016). Hashimoto encephalopathy: literature review. *Acta Neurologica Scandinavica*, *135*(3), 285–290. https://doi.org/10.1111/ane.12618

Zhu, C., Herrmann, U. S., Falsig, J., Abakumova, I., Nuvolone, M., Schwarz, P., Frauenknecht, K., Rushing, E. J., & Aguzzi, A. (2016). A neuroprotective role for microglia in prion diseases. *Journal of Experimental Medicine*, *213*(6), 1047–1059. https://doi.org/10.1084/jem.20151000

Tables

Table 1. Systematic survey of public human prion-disease expression series. Seven query formulations returned 60 unique records; 15 passed disease-relevance screening; 10 are genuine human prion-disease series.

Accession	n	Assay	Material	Disposition
GSE124571	21	Expression array	sCJD frontal cortex	Reanalysed
GSE160208	47	NanoString, 800-gene panel	sCJD cortex + cerebellum	Reanalysed, 3 contrasts
GSE140069	105	Small RNA-seq	sCJD whole blood	Reanalysed; cited from qPCR
GSE156994	219	450K methylation	sCJD whole blood	Published DMPs cited
GSE330903	31	RNA-seq	LN229 / GM12878, PRNP depletion	Reanalysed
GSE214373	14	RNA-seq	sCJD frontal cortex	Cannot adjudicate — quality gradient
GSE214374	26*	Single-nuclei RNA-seq	Prion disease brain	Cannot adjudicate — depth
GSE214376	35	SuperSeries	Human + mouse	Parent series
GSE40562	8	Expression array	FFI thalamus / parietal	Insufficient controls (n = 2)
GSE30643	2	Expression array	Genetic CJD parietal cortex	Insufficient (n = 2)

Table 2. Independent lines of evidence converging on FKBP5 and CDKN1A. The two prior candidate sets are enumerated in Section 3.2; FKBP5 is the only member of their intersection.

Gene	Layer	Evidence	Source
FKBP5	Blood methylation	Promoter hypomethylation; 1 of 4 loci surviving composition correction and replicating by pyrosequencing (n = 186)	Dabin 2020
FKBP5	Endocrine	Serum cortisol difference	Dabin 2020

		147.9 nM (95% CI 77.8–218.1; $p = 6.6\times10^{-5}$); text and figure legend disagree on direction, see Section 3.2	
FKBP5	Brain protein network	1 of 10 hub proteins; independent analysis, same two series	Mredul 2022
FKBP5	Brain transcript	+1.03 (FDR 0.0022), frontal cortex	This study
FKBP5	Brain transcript	+0.95 cortex; +1.68 cerebellum (both FDR < 0.05)	This study
CDKN1A	Brain protein network	Hub protein; independent analysis, same two series	Mredul 2022
CDKN1A	Blood miRNA target	De-repressed miR-93-5p target	Norsworthy 2020
CDKN1A	Brain transcript	+2.18 cortex; +2.54 cerebellum	This study

Table 3. Cross-cohort replication of the brain transcriptome, GSE124571 against GSE160208.

Comparison	**Genes**	**Statistic**	**Stability**
All shared genes	750	Pearson r = 0.684	—
Significant in both	143	Pearson r = 0.843	Bootstrap 95% CI 0.783–0.887
Significant in both	143	Spearman r = 0.730	Leave-one-out 0.834–0.857
Directional agreement	143	142 / 143 (99.3%)	—
Cortex vs cerebellum	800	Pearson r = 0.821	248 / 252 same direction

Table 4. The four replicated blood-methylation loci of Dabin et al., tested in sCJD brain (GSE124571). Detection is the number of samples with a detection p-value below 0.01.

Locus	**Blood methylation signal**	**Probes on array**	**Detection**	**Brain log2FC**	**FDR**
FKBP5	Promoter hypomethylation	1	21/21	+1.03	0.0022
AIM2	Hypomethylation, 2 probes; tracks MRC decline	1	0/21	below detection	—
UHRF1	Replicated by pyrosequencing	1	0/21	below detection	—
KCNAB2	Replicated by pyrosequencing	2	12/21 and 17/21	−0.22 and −0.30	0.069 and 0.067

Table 5. The glucocorticoid receptor chaperone complex in sCJD frontal cortex (GSE124571). Probe identifiers omit the ILMN_ prefix. The final row is the within-sample log2 ratio of the two affinity-setting co-chaperones. NR3C1 lies close to the detection floor on this platform and its value should not be read as evidence of preserved receptor abundance; HSP90AA1 carries a second, more abundant probe (2373515) giving +0.20 at p = 0.11. Both points are set out in Section 3.4.

Gene	**Protein**	**Role at the receptor**	**Probe**	**log2FC**	**FDR**
NR3C1	GR	The receptor itself (near detection floor)	2389347	−0.14	0.081
HSP90AA1	Hsp90α	Scaffold	1687546	+0.71	0.005
STIP1	HOP	Complex assembly	1789510	+0.29	0.059
FKBP4	FKBP52	Raises hormone avidity; recruits dynein	1782045	+0.21	0.273
FKBP5	FKBP51	Lowers hormone-binding affinity	1778444	+1.03	0.0022

FKBP1A	FKBP12	Tacrolimus target; not a GR co-chaperone	2333367	−0.83	0.059
FKBP10	FKBP65	ER lumen; PrP^c biogenesis	1659905	below detection	—
FKBP5 − FKBP4	—	Inhibitory : stimulatory ratio	—	−0.63 → +0.19 (+0.82)	Welch p 0.0043

Table 6. Gene-set response to glial activation in GSE124571 (21 samples), computed from the raw intensity file. Slope is given per unit of microglial score. Two adjusted quantities are reported because they are not equivalent: the coefficient on group in a model fitting group and the microglial score simultaneously, which is the estimand used for single probes, and the group difference in residuals after regression on the score alone, which earlier drafts reported. They agree in sign throughout.

Gene set	**Genes**	**Group difference (z)**	**Slope on glial score**	**Adjusted coefficient**	**Residual difference**
Microglial markers	7	+1.26	—	—	—
Neuronal / synaptic	4	−1.19	−0.76	−0.44 (p 0.30)	−0.24 (p 0.43)
NF-κB targets	9	+1.09	+0.76	+0.24 (p 0.33)	+0.13 (p 0.45)
Inflammasome effectors	4	+1.19	+0.97	−0.04 (p 0.83)	−0.02 (p 0.87)
Inflammasome sensors (NLRP3)	1	−0.29	+0.32	—	−0.70 (p 0.10)
NRF2 targets	6	+1.19	+0.77	+0.42 (p 0.10)	+0.23 (p 0.21)
Ferroptosis	2	−0.72	−0.47	−0.25 (p 0.60)	−0.13 (p 0.70)

Table 7. FKBP5 in GSE160208 stratified by sex. The cohort is sex-balanced by design and FKBP5 is elevated within each stratum. In the final row the two groups are female and male controls, not control and patient, with observations from both regions pooled; because each donor contributes two regions, that row is descriptive and is not a test of a disease-by-sex interaction, which these data are not powered to provide.

Region	**Stratum**	**Group 1 n**	**Group 2 n**	**Welch t**
Frontal cortex	All	10	14	3.91
Frontal cortex	Males	5	7	2.69
Frontal cortex	Females	5	7	2.88
Cerebellum	All	10	13	3.91
Cerebellum	Males	5	7	3.24
Cerebellum	Females	5	6	2.32
Both, pooled	Control females vs males	10	10	−0.10 (ns)

Table 8. FKBP5 does not respond to PRNP depletion (GSE330903, LN229 cells, representative doses).

Condition	**Δ PRNP**	**Δ FKBP5**
CP3, 10,000 nM	−1.86	−0.32
CP3, 31,600 nM	−1.83	+0.09
CP3 + BPN, 3,160 nM	−1.72	−0.19
SMSM74, 31,600 nM	−1.69	−0.27
Risdiplam, 31,600 nM	−0.37	−0.35
PRNP–FKBP5 correlation, all 25 samples	r = +0.241 (p = 0.25)	48.2nd percentile of 23,102 genes

Table 9. Predicted ADMET properties. TPSA, topological polar surface area. Tacrolimus is a known false negative for predicted penetration and is included as a control.

Compound	**MW**	**TPSA**	**Lipinski**	**BBB**	**hERG**	**Composite**
Phloroglucinaldehyde	154.1	77.8	pass	yes	0.00	0.814

(metabolite)						
Protocatechuic acid (metabolite)	154.1	77.8	pass	yes	0.00	0.809
Resveratrol	228.3	60.7	pass	yes	0.10	0.727
Ferrostatin-1	262.4	64.4	pass	yes	0.42	0.671
Delphinidin-3-O-glucoside	465.4	211.8	fail	no	0.00	0.475
Cyanidin-3-O-glucoside	449.4	191.6	fail	no	0.00	0.468
Malvidin-3-O-glucoside	493.4	189.8	fail	no	0.00	0.457
Tacrolimus (control)	804.0	178.4	fail	no	0.41	0.277

Table 10. FKBP5 across a graded CNS-infection severity series (GSE35864, frontal cortex), with sCJD values for comparison. Expression on the log2 scale.

Group / gene	**n**	**FKBP5 (log2)**	**Difference vs control**	**sCJD equivalent**
Uninfected control	6	7.50	—	—
HIV, no impairment	6	7.56	+0.06	—
HIV-associated dementia	7	7.77	+0.27	—
HIV encephalitis	5	7.82	+0.32 (FDR 0.20)	+1.03 (FDR 0.0022)
Trend with severity	24	Spearman rho 0.36	GFAP rho 0.40, same samples	—
TLR4	—	—	+0.64	+0.44
NFE2L2	—	—	+0.59	+0.53
CDKN1A	—	—	+0.75	+1.12
BDNF	—	—	−0.67	−0.65
PRNP	—	—	−0.95	−1.11

Table 11. Human and prion-model evidence bearing on host-response modulation, grouped by what each line of evidence addresses. Dashes mark outcomes the study did not assess.

Evidence	**Setting**	**Survival**	**Clinical or pathological effect**	**Source**
Corticosteroid pulse	Definite sCJD, case report	—	Seizures aggravated: generalised myoclonus, epilepsia partialis continua, ballistic dyskinesia	(Jang et al., 2014)
Short-course glucocorticoid	RT-QuIC-confirmed CJD, case report	—	3 days improvement, then rapid decline within a week	(Wu et al., 2025)
Glucocorticoids, 23 of 64 patients	CJD series, abstract only	No difference	—	(Sarandria, 2025)
Corticosteroids	Confirmed human CJD	No trial or cohort study identified	—	this survey
Dexamethasone, 5 nM, 72 h	Primary microglia	—	Phagocytosis reduced; senescence-like, not reversed by washout	(Park et al., 2019)
Prednisone, prophylactic	Mouse scrapie, peripheral route	Reduced susceptibility	—	(Outram et al., 1974)
Anti-inflammatory treatment	Mouse scrapie, peripheral route	Incubation prolonged	—	(Outram et al., 1975)
FK506 from day 20 p.i.	Mouse, Fukuoka-1 prion	Prolonged	PrP^{sc} reduced; LC3-II up	(Nakagaki et al., 2013)
Calcineurin inhibition at clinical phase	Mouse, prion-infected	Prolonged	PrP^{sc} unchanged	(Mukherjee et

				al., 2010)
Oral FK506 at or after onset	Knock-in human PrP, sCJD prions	Prolonged (modest)	Gliosis suppressed	(Nakagaki et al., 2020)
FK506 + minocycline, symptomatic	Hamster, prion-infected	—	GFAP/IBA-1 and NF-κB down; NRF2–HO-1 up	(Shah et al., 2019)
Microglial ablation; IL-34 deficiency	Slice culture and mouse	Accelerated	PrP deposition increased	(Zhu et al., 2016)
CSF-1R inhibition, 78–90% depletion	Mouse, RML / ME7 / 22L	Accelerated by 31 d (RML, early) and 33 d (RML, 80 dpi)	PrP^{sc} and vacuolation increased	(Carroll et al., 2018)
Microglia-deficient Csf1r enhancer deletion	Mouse, prion-infected	Accelerated	PrP accumulation lower; astrocytosis earlier	(Bradford et al., 2022)
Systemic endotoxin challenge	Mouse ME7 prion	Earlier onset of impairment	Exaggerated IL-1β / TNF-α / IFN-β; neuronal apoptosis	(Cunningham et al., 2009)

Figure legends

Figure 1. Study workflow. Stage 1, systematic identification of eligible Gene Expression Omnibus series. Stage 2, per-dataset processing; GSE124571 (amber) was re-processed from raw deposited intensities, the remaining series were analysed from submitter-deposited matrices, and GSE35864, which is not a prion dataset, enters as a comparator series rather than through the prion disease screen. Stage 3, analyses; the candidate-locus test is marked to show that the candidate set was fixed before any analysis on brain-derived samples was run. Stage 4, mapping of analyses onto main-text and supplementary display items.

Figure 2. Cross-cohort replication of the brain transcriptome. Log_2 fold change in GSE124571 plotted against GSE160208 frontal cortex for the 143 genes reaching FDR < 0.05 in both cohorts, drawn from the 750 panel genes carrying a probe on the genome-wide array. Orange line, least-squares fit; grey dashed line, identity. Pearson r = 0.843 (bootstrap 95% CI 0.783–0.887); 142 of 143 genes agree in direction (99.3%). Across all 750 shared genes r = 0.684. All values are computed from the deposited raw intensity file by the pipeline in Supplementary Software.

Figure 3. FKBP5 is glia-associated but does not behave like a gliosis marker. (A) The group effect for FKBP5 and five anchor genes before and after adjustment for the microglial score. GFAP, C1QB, SERPINA3 and CDKN1A lose most of their effect; FKBP5 retains half of its own. (B) The distribution of absolute composition-adjusted group effects among the 332 probes whose correlation with the microglial score is at least as strong as FKBP5's. The peer median is 0.11; FKBP5 is 0.53, ranking 12th of 332. No probe in the dataset retains an adjusted effect at FDR below 0.05, so these are rankings, not significance claims. (C) Group effect for the thirteen canonical glucocorticoid-receptor target transcripts measured above background, ordered by each target's correlation with the microglial score (given in brackets). The six above the dotted line are glia-associated and five of them reach FDR < 0.05; the seven below it, including TSC22D3 and DUSP1, are unchanged. Across the thirteen the group effect tracks glial correlation at r = 0.80.

Figure 4. FKBP5 does not respond to PRNP depletion. (A) FKBP5 against PRNP across the 25 GSE330903 samples, with vehicle controls marked separately; splice-switching compounds deplete PRNP by up to 1.9 log_2 units without moving FKBP5 (r = +0.241, p = 0.25). (B) The distribution of PRNP correlations for all 22,805 expressed genes, with FKBP5 marked at the 48th percentile; the percentile lies between 47 and 49 under every per-sample detection filter tried. These are non-neural, uninfected cell lines, so the comparison addresses PrP^{c} abundance rather than PrP^{sc} burden.

Figure 5. Specificity of the blood miRNA signature depends on normalisation. Each of the 194 analysed miRNAs is plotted by its effect-size percentile against all others, under counts-per-million (x) and median-of-ratios (y) normalisation. The three previously reported miRNAs sit near the 5th percentile under one scheme and near the 50th under the other. Only miR-106b-5p is an outlier under both.

Figure 6. FKBP5 across a graded CNS-infection series. (A) Individual samples and group means for FKBP5 in frontal cortex across the GSE35864 severity gradient; the dashed line joins the group means. Expression increases with severity (Spearman rho = 0.36). (B) The effect at the severe end of that gradient set beside the sCJD effect measured here, on the same log_2 scale: HIV encephalitis reaches +0.32 against +1.03 in sCJD, a little under a third. The two series were assayed on different platforms and processed independently, so the comparison is indicative only, not quantitative.

Figure 7. Predicted pharmacokinetics separate the parent anthocyanins from their metabolites. Composite ADMET score against topological polar surface area for the eight compounds in Table 9, coloured by predicted blood–brain barrier penetration. The shaded band marks the transitional range of topological polar surface area, 130–170 $Å^2$, within which prediction is least reliable. Tacrolimus (triangle) is a known false negative in this model and is included as a control, so predicted non-penetrance should be read as suggestive rather than decisive.

Figure 8. The glucocorticoid receptor complex in sCJD frontal cortex (GSE124571). (A) Log_2 fold changes for the glucocorticoid receptor and the components of its heterocomplex, with the fold change and FDR tabulated at the right of the panel; bars are filled solid where FDR is below 0.05 and left pale otherwise. The inhibitory co-chaperone rises furthest. NR3C1 is shown for completeness but lies near the detection floor on this platform, so its bar carries no weight, and the two HSP90AA1 probes disagree (Section 3.4). FKBP1A is set below the rule because FKBP12 is a target of FK506 and not a component of the glucocorticoid receptor heterocomplex; it is carried here only as a specificity control, to show that the FKBP family does not move as a block. (B) The within-sample log_2 ratio of FKBP5 to FKBP4 across the 21 samples, which inverts from FKBP52-dominant in controls to FKBP51-dominant in sCJD. The shift is +0.82; as Section 3.4 sets out, its nominal p-value adds nothing to the two marginal effects and is not quoted here. Horizontal bars mark group means, annotated with their values.

Figures

Figure 1

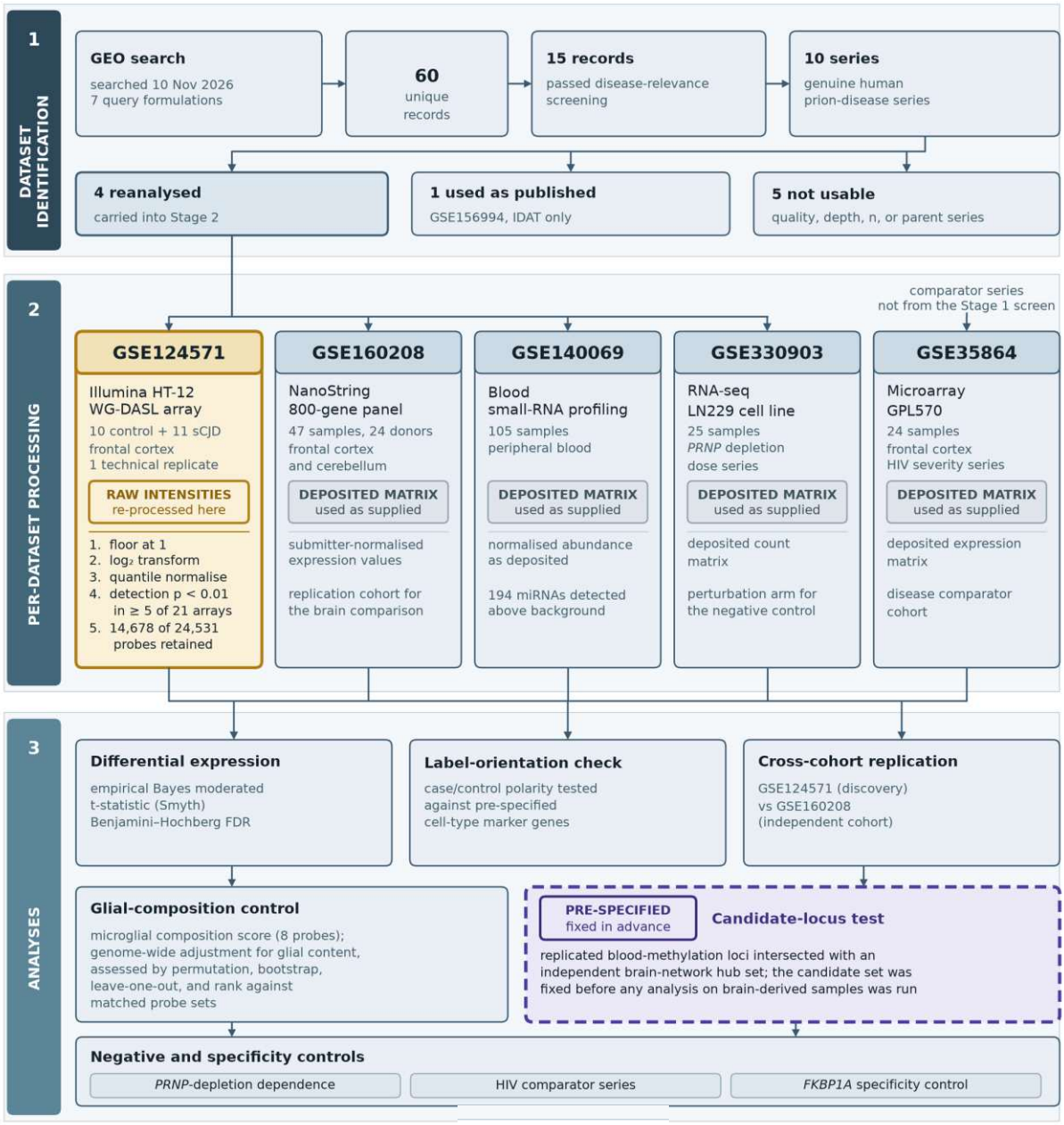


Figure 2

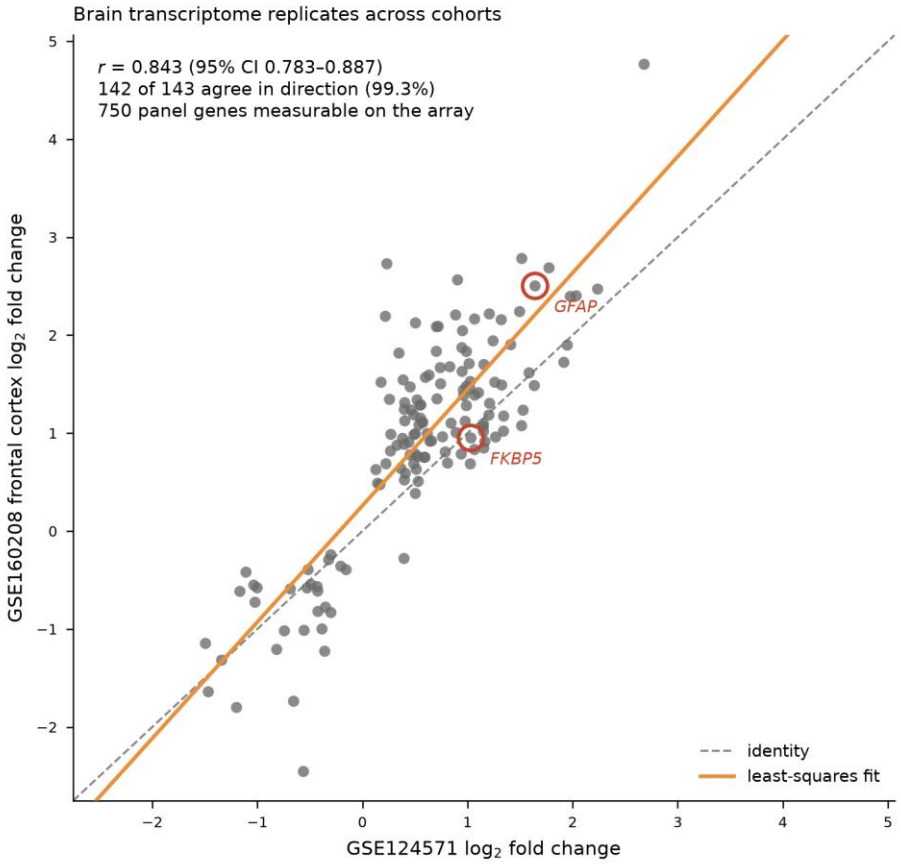

Brain transcriptome replicates across cohorts
r = 0.843 (95% CI 0.783–0.887)
142 of 143 agree in direction (99.3%)
750 panel genes measurable on the array
GFAP
FKBP5
identity
least-squares fit
GSE160208 frontal cortex log2 fold change
GSE124571 log2 fold change
5
4
3
2
1
0
−1
−2
−2
−1
0
1
2
3
4
5

Figure 3

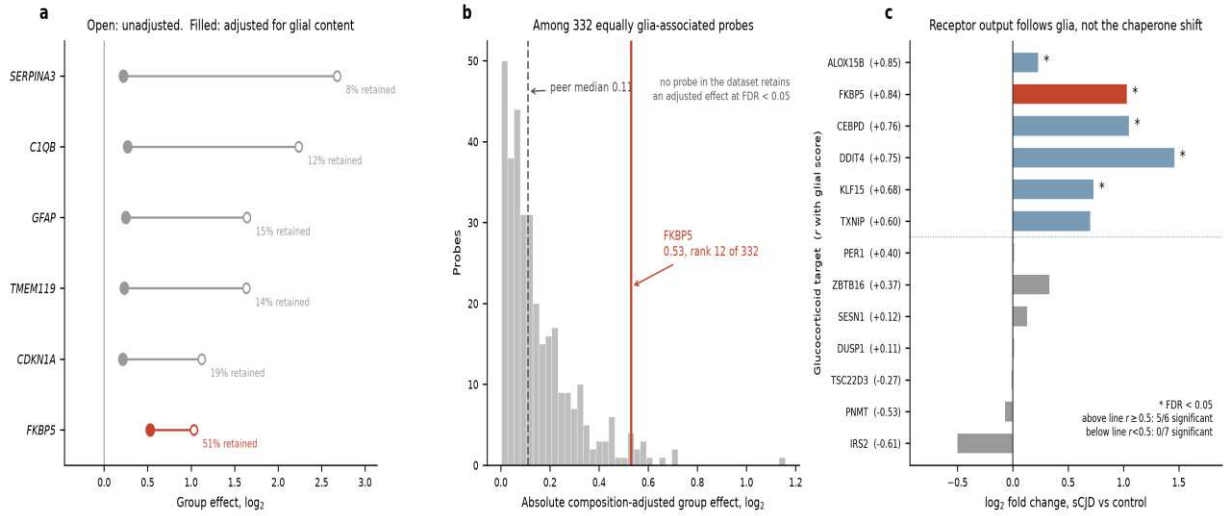

a
Open: unadjusted. Filled: adjusted for glial content
SERPINA3
8% retained
C1QB
12% retained
GFAP
15% retained
TMEM119
14% retained
CDKN1A
19% retained
FKBP5
51% retained
0.0 0.5 1.0 1.5 2.0 2.5 3.0
Group effect, log2
b
Among 332 equally glia-associated probes
peer median 0.11
no probe in the dataset retains an adjusted effect at FDR < 0.05
FKBP5
0.53, rank 12 of 332
Probes
0 10 20 30 40 50
0.0 0.2 0.4 0.6 0.8 1.0 1.2
Absolute composition-adjusted group effect, log2
c
Receptor output follows glia, not the chaperone shift
Glucocorticoid target (r with glial score)
ALOX15B (+0.85) *
FKBP5 (+0.84) *
CEBPD (+0.76) *
DDIT4 (+0.75) *
KLF15 (+0.68) *
TXNIP (+0.60)
PER1 (+0.40)
ZBTB16 (+0.37)
SESN1 (+0.12)
DUSP1 (+0.11)
TSC22D3 (-0.27)
PNMT (-0.53)
IRS2 (-0.61)
* FDR < 0.05
above line r ≥ 0.5: 5/6 significant
below line r<0.5: 0/7 significant
−0.5 0.0 0.5 1.0 1.5
log2 fold change, sCJD vs control

Figure 4

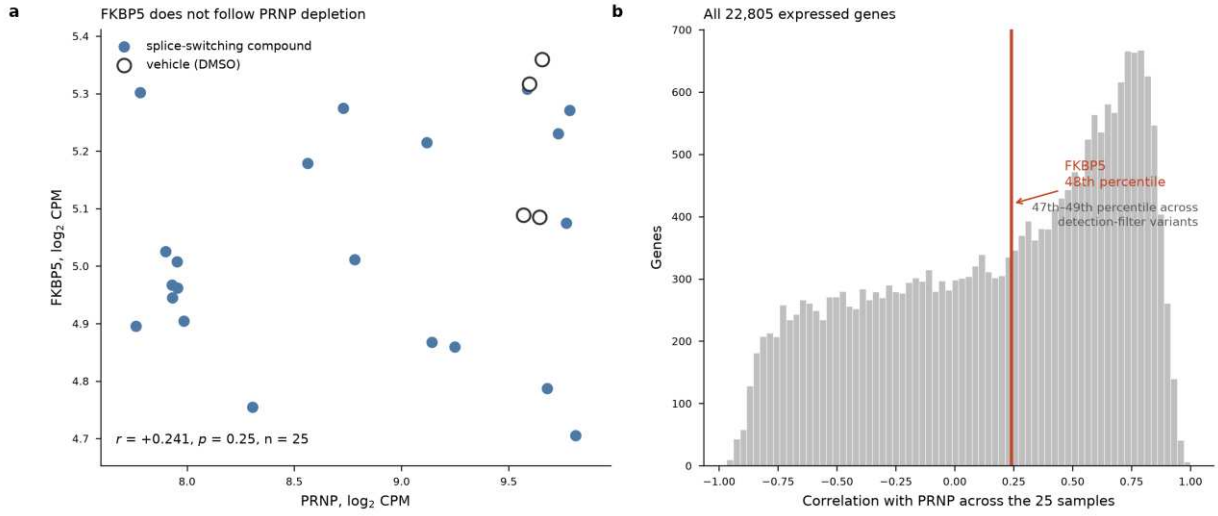

a
FKBP5 does not follow PRNP depletion
splice-switching compound
vehicle (DMSO)
FKBP5, log2 CPM
PRNP, log2 CPM
r = +0.241, p = 0.25, n = 25
b
All 22,805 expressed genes
Genes
FKBP5
48th percentile
47th–49th percentile across
detection-filter variants
Correlation with PRNP across the 25 samples

Figure 5

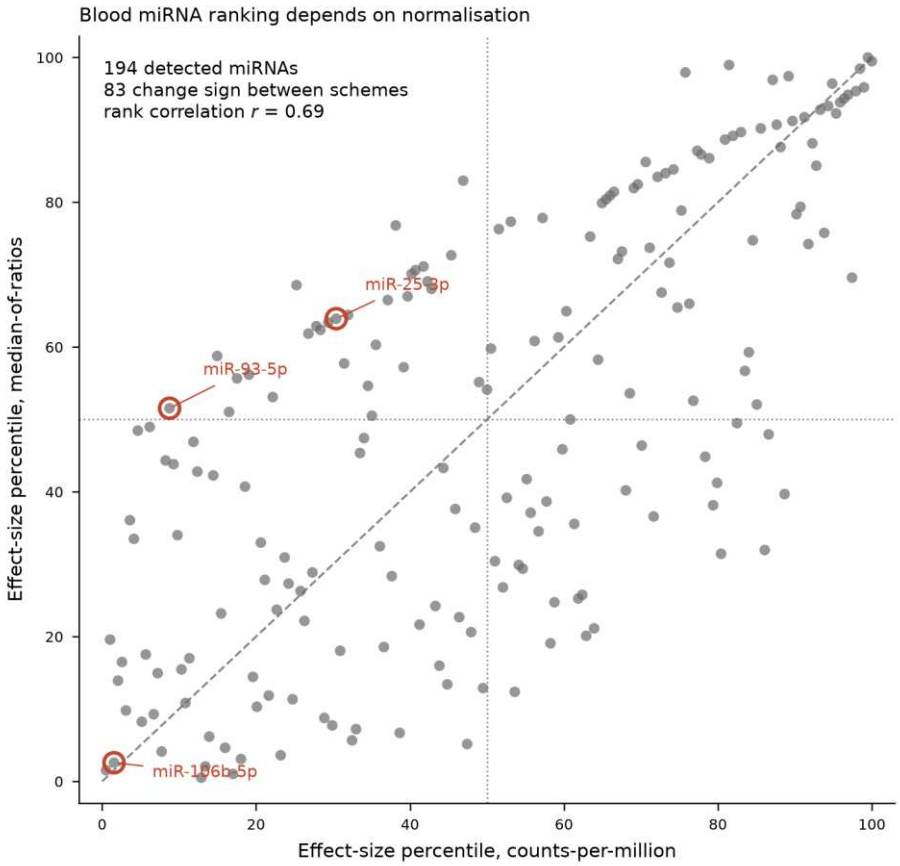

Blood miRNA ranking depends on normalisation
194 detected miRNAs
83 change sign between schemes
rank correlation r = 0.69
miR-25-3p
miR-93-5p
miR-106b-5p
Effect-size percentile, median-of-ratios
Effect-size percentile, counts-per-million
0
20
40
60
80
100

Figure 6

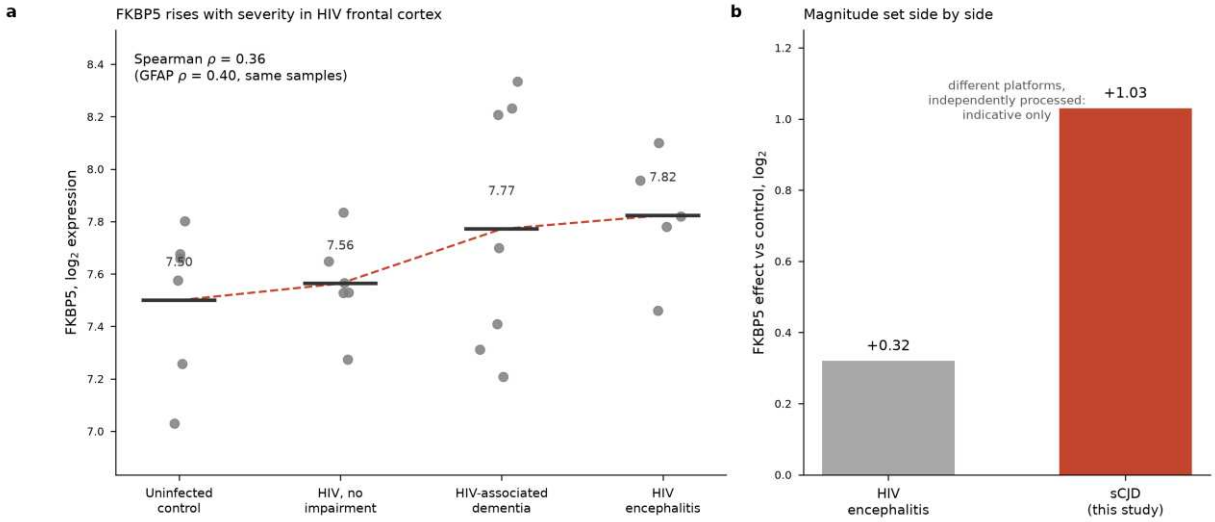

a
FKBP5 rises with severity in HIV frontal cortex
Spearman ρ = 0.36
(GFAP ρ = 0.40, same samples)
FKBP5, log2 expression
8.4
8.2
8.0
7.8
7.6
7.4
7.2
7.0
7.50
7.56
7.77
7.82
Uninfected control
HIV, no impairment
HIV-associated dementia
HIV encephalitis
b
Magnitude set side by side
FKBP5 effect vs control, log2
1.2
1.0
0.8
0.6
0.4
0.2
0.0
different platforms, independently processed: indicative only
+1.03
+0.32
HIV encephalitis
sCJD (this study)

Figure 7

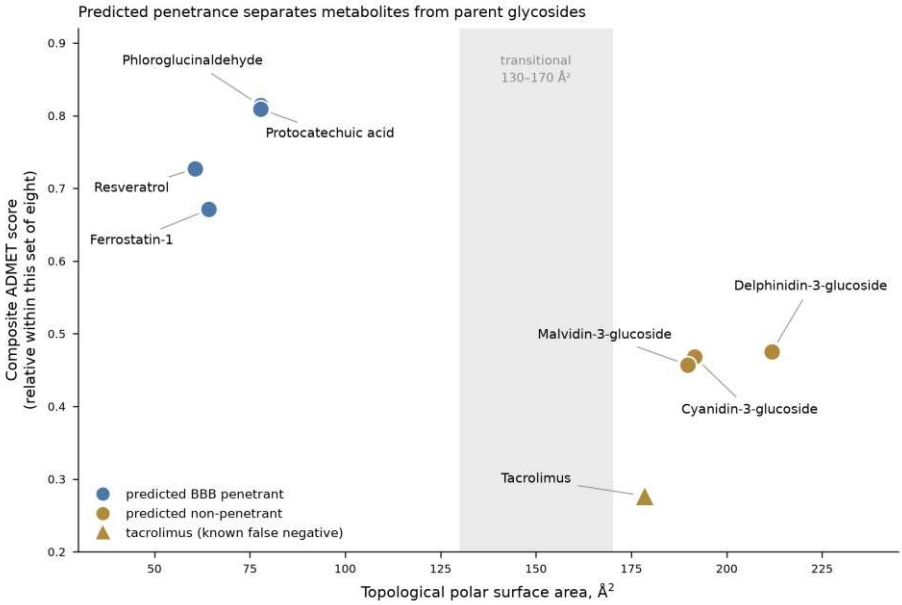
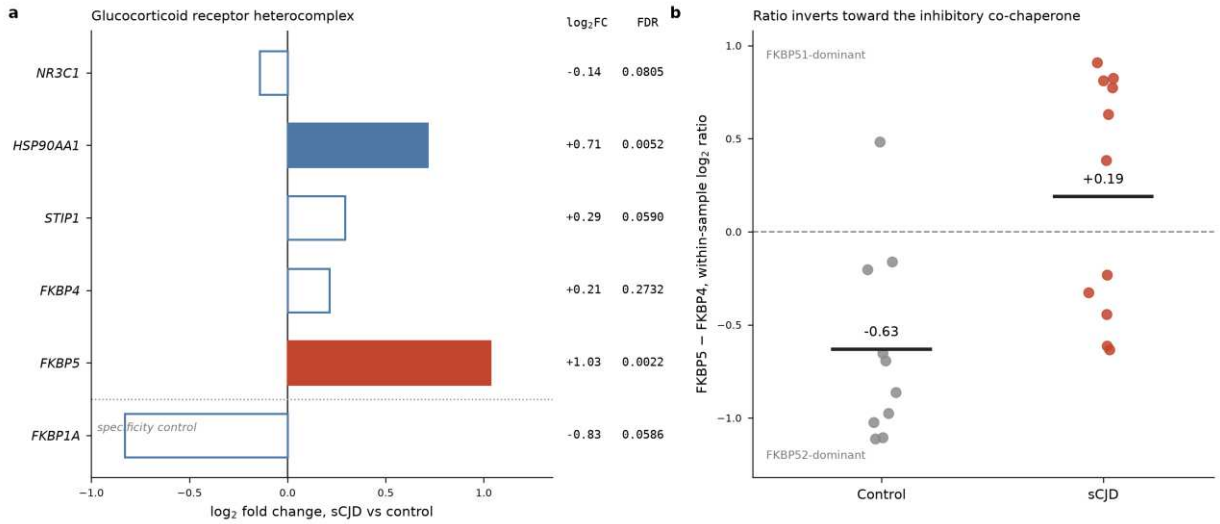

Predicted penetrance separates metabolites from parent glycosides
Phloroglucinaldehyde
Protocatechuic acid
Resveratrol
Ferrostatin-1
transitional
130–170 Å²
Delphinidin-3-glucoside
Malvidin-3-glucoside
Cyanidin-3-glucoside
Tacrolimus
predicted BBB penetrant
predicted non-penetrant
tacrolimus (known false negative)
Composite ADMET score
(relative within this set of eight)
Topological polar surface area, Å²
0.9
0.8
0.7
0.6
0.5
0.4
0.3
0.2
50
75
100
125
150
175
200
225

Figure 8


a
Glucocorticoid receptor heterocomplex
log2FC
FDR
NR3C1
-0.14
0.0805
HSP90AA1
+0.71
0.0052
STIP1
+0.29
0.0590
FKBP4
+0.21
0.2732
FKBP5
+1.03
0.0022
FKBP1A
-0.83
0.0586
specificity control
−1.0
−0.5
0.0
0.5
1.0
log2 fold change, sCJD vs control
b
Ratio inverts toward the inhibitory co-chaperone
FKBP51-dominant
FKBP52-dominant
FKBP5 − FKBP4, within-sample log2 ratio
1.0
0.5
0.0
−0.5
−1.0
+0.19
-0.63
Control
sCJD